

EQC Project 14/662

Improved understanding of liquefaction effects on shallow foundations for enhanced aseismic design

Nawawi Chouw, Rolando Orense, Gonzalo Barrios and Tam Larkin
Department of Civil and Environmental Engineering
The University of Auckland

December 2017



**THE UNIVERSITY
OF AUCKLAND**

NEW ZEALAND

Te Whare Wānanga o Tamaki Makaurau

CONTENTS

1	Introduction.....	4
1.1	Structure-footing-soil (SFS) system	4
1.2	Research objectives	4
2	Laminar box.....	5
2.1	Design criteria.....	5
2.2	Large laminar box for saturated sand	6
2.2.1	Base and Barriers	7
2.2.2	Laminar Layers	8
2.2.3	Membrane.....	9
2.2.4	Preparation of the sand specimen.....	11
2.3	General set-up of the large laminar box	12
3	Influence of soil on the response of a SDOF structure with a shallow footing	16
4	Subsurface behaviour of saturated sand and the effects of shallow footings	21
4.1	Introduction	21
4.2	Methodology.....	22
4.2.1	Soil properties	23
4.2.2	Instrumentation.....	24
4.2.3	Footing models.....	24
4.2.4	Tests configurations	25
4.2.5	Ground motions.....	25
4.3	Results and discussion.....	26
4.3.1	Free-field	26
4.3.2	Effects of footings	35
5	Conclusions.....	41
6	Recommendations.....	43
7	Publications and public dissemination.....	44
7.1	PhD theses	44
7.2	Journal articles.....	44
7.3	Conference papers	44
7.4	Knowledge transfer through teaching activities	44
7.5	Public seminars.....	45
	References	46

SUMMARY

This report concerns a series of experiments carried out to investigate the earthquake response of a system involving the foundations and the supporting saturated sand. A large laminar box was designed and constructed to simulate the passage of earthquake waves through the saturated sandy soil. The box was placed on a large shake table which provided the excitations. The response of the soil was closely monitored using a variety of instrumentation and the data analysed to enable an understanding of the predominant features of the response of the system.

The philosophy behind the design and the method of construction of the laminar box are described and the method of preparing and saturating the sand outlined. An initial series of experiments utilising a simple instrumented structure on dry sand was carried out as a verification of the functioning of the laminar box, i.e. if it was suitable for the purpose. The response of the structure was compared with theoretical solutions available in the literature. This work throws light on the role of soil-structure interaction in earthquake response, which is often ignored in usual design practice.

A major part of the work presented here concerns the response of a body of saturated sand to a series of ramped harmonic loadings, all with an amplitude of 0.2g but with 3 different frequencies: 1, 1.5 and 2 Hz. The response of the sand without the presence of footings was first explored. This was followed by studies of a system comprising of a single footing and a more complex system of a cluster of 6 closely adjacent footings. All footings were mounted on the surface of the saturated sand. The sand and footings were extensively instrumented to record excess pore water pressure, acceleration of the sand and the footings, relative lateral displacement at three elevations and vertical displacement of both the sand surface and the footings.

The results are herein discussed and the most important features are presented that lead to an improved understanding of liquefaction effects on shallow foundations including the nature of the soil and footing response to the different types of loading. From this information, conclusions and a series of recommendations are made that will be of use to designers.

ACKNOWLEDGMENTS

Grateful thanks are extended to the Earthquake Commission for Grant Number 14/662 that allowed the work to proceed.

The authors would like to acknowledge the significant contribution of many graduate and undergraduates student during the protracted course of this work.

1 INTRODUCTION

1.1 Structure-footing-soil (SFS) system

During an earthquake, the movement of soil causes movement of structures and this structural response, in turn, influences the movement of soil. This structure-footing-soil interaction (SFSI) can cause the seismic response of a structure to be different from that of an identical structure with an assumption of an idealised fixed base. This process will likely cause the response of the soil to be different from what would be measured under a free-field condition, i.e. with an absence of the structure. Observations from major earthquakes, including those from the 2010-2011 Canterbury earthquakes, have identified significant influences that the behaviour of soil can have, on the overall seismic performance of SFS systems.

By performing physical experiments, a more realistic simulation of the structural response with SFSI can be achieved, since analytical and numerical simulations will never be able to describe the actual nonlinear behaviour of SFS systems accurately, simply because of the assumptions made. Physical experiments with a shake table allow researchers to not only understand the effects of SFSI, but they also enable a validation and an improvement of numerical and analytical models. An early contribution to the understanding of SFSI was presented by Taylor et al. (1980), where cyclic displacements were applied to a number of model footings seated on clay and sand. The results suggested that the soil beneath the footing can be intentionally designed to deform well into the nonlinear range in strong earthquakes. This nonlinear soil behaviour can activate rigid-like body movements of the structure. As a consequence, development of a plastic hinge in the structure could be avoided. As discussed by Veletsos and Meek (1974), the flexible ground can act as a damper by absorbing a large part of the vibration energy arising from earthquakes and thus can reduce the seismic response of a structure. Larkin (2008) also concluded that the flexibility of the supporting soil can lengthen the vibration period of the structure-footing-soil system, and result in a variation of structural response when compared to those obtained from analyses that do not consider SFSI.

The foundations in this study were placed on the surface of the sand. In practice, individual foundations are usually embedded, i.e. placed below the surface. This induces an increased confining stress on the load carrying volume of soil and hence reduces settlement and the risk of bearing failure. The excavation of a cavity in the soil will induce kinematic interaction. For the majority of shallow foundations this feature of SSI is thought to be relatively small compared with inertial interaction. Thus the observations and conclusion from this study are thought to also apply to the majority of shallow foundations.

1.2 Research objectives

The research focuses on an understanding of the effect of liquefaction on shallow foundations and will elucidate the development of failure of coupled soil-shallow foundation systems in liquefied soil.

The research has the following objectives:

1. Design and construction of a large-scale laminar box of $2\text{ m} \times 2\text{ m} \times 2\text{ m}$ for investigating the behaviour of shallow foundations in a liquefied soil involving one dimensional horizontal motion
2. Synthesis of the experimental and numerical results to explain the process leading to liquefied soil-shallow foundation response
3. Formulation of design recommendations for shallow foundations
4. Presentation and dissemination of the research outcomes at national and international platforms
5. Implementation of the research by educating future engineers and by enhancing the understanding of practicing engineers.

2 LAMINAR BOX

2.1 Design criteria

Experimental simulation of the structural response, including partial and temporary separation at the interface between footing and the supporting soil, depends on the laboratory replication of soil response during earthquakes that is close to reality. This can be achieved through the use of a laminar box. Laminar boxes are designed to simulate in situ soil conditions under seismic loading; that is to allow the soil to undergo predominantly shear deformation during a shake table test.

Some of the characteristics that make laminar box tests preferable to other experimental approaches, e.g. field tests, are as follows (X. Qin 2016):

1. The ability to closely simulate the boundary conditions of *in situ* soil.
2. The capacity to test soil specimens that are larger than the ones used in conventional laboratory element experiments, such as triaxial tests which typically have a specimen height of 300 mm or less.
3. Being able to explore the behaviour of soil in non-uniform, partially drained, layered, and sloping sites.
4. The ability to reproduce the response of a structure and soil as one holistic system.

To enable more realistic soil behaviour under dynamic load a laminar box has been constructed by a number of researchers. Such a box has the advantage that it can simulate appropriate boundary conditions considerably better than a rigid box. The laminar box generally consists of a horizontal stack of rectangular frames separated by linear roller bearings arranged to permit relative movement between frames in the horizontal plane with minimal friction. Laminar boxes in general are designed to permit an overall shear strain in the soil deposit of up to 20%. These large strains are provided to accommodate post liquefaction-induced soil lateral deformation. Most of the boxes are made of high strength aluminium alloy.

Researchers have designed various types of laminar boxes in the past. A very simple laminar box was utilised by Latha and Krishna (2008). In their study the small box was rectangular in plan with internal dimensions of 0.5 m × 1 m × 0.8 m. The box consisted of 15 laminar layers, constructed from pieces of hollow aluminium rectangular sections. The layers were separated by linear roller bearings to minimise friction. A more complicated laminar box was described by Ueng et al. (2005). This box was designed to undergo two-axis shaking and hence was called a biaxial laminar box. The box was rectangular in plan and had internal dimensions of 1.88 m × 1.88 m × 1.52 m. It was made up of 15 horizontal layers and had a special sliding system which allowed movements in the horizontal plane. The layers were supported by a rigid steel structure which surrounded the entire box. The inside of this biaxial box was sealed with a 2 mm thick silicone rubber membrane which allowed for the testing of both dry and wet soils.

Considering laminar boxes worldwide, most can only be used for dry sand, e.g. at the University of Bristol, Pitilakis et al. (2008) in UK (1.19 m × 0.55 m × 0.814 m), at the University of Western Ontario, Turan et al. (2009) in Canada (0.45 m × 0.9 m × 0.807 m), at the Indian Institute of Science in Bangalore in India, Madhav and Krishna (2008) (0.5 m × 1 m × 0.8 m), at the University of Tokyo, Prasad et al. (2004) in Japan (0.5 m × 1 m × 1 m) and the small box constructed at the University of Auckland (Cheung, et al. 2013, Qin, et al. 2013) in the Department of Civil and Environmental Engineering. A laminar box capable of simulating liquefied sand undergoing large deformation is not only much more complex to build but also requires more types of measurement devices.

To date only a few boxes capable of simulating liquefied sand have been reported, e.g. the one at the National Taiwan University (Ueng 2010), National Centre for Research on Earthquake Engineering in Taipei, where the box size is 1.88 m × 1.88 m × 1.52 m. The other previous facility known to the authors as capable of reproducing the conditions necessary for this study is the defunct large scale box of the National Research Institute for Earth Science and Disaster Prevention (NIED) in Tsukuba, Japan. The box was 12 m long, 3.5 m wide and 6 m high and was used extensively for the Earthquake Damage to Underground Structures project in the 1990s (Mori, et al. 1997, Orense, et al. 2001, Yasuda, et al. 2000). This was replaced by the large-scale cylindrical laminar container of 8 m diameter and 6.3 m height at the E-Defence facility in Miki, Japan, which used the largest shake table in the world. However, the cost is prohibitive, being approximately half a million US dollars per test. Sato and Tabata (2010) of NIED reported a comparative study of the effect of soil liquefaction and concluded that using a tiny laminar box in a centrifuge test is insufficient to reproduce the results from E-Defence, although the agreement improved when the diameter of the comparatively tiny laminar container was increased from 0.3 m to 0.4 m. This research shows that this and similar studies cannot reasonably be undertaken on a centrifuge. Furthermore, this Japanese study suggests that our existing small laminar box is suitable for parametric studies only. The detailed study completed in this EQC research needs to be carried out using a much larger laminar box than is possible in most centrifuge experiments to take into account effective stresses in the range of those encountered in the field.

While Japanese colleagues have performed some preliminary tests involving the influence of liquefied soil on harbour structures (Motamed, et al. 2013), we are aware of only very limited testing on shallow foundations, e.g. in National Institute for Earth Science and Disaster Prevention in Tsukuba in Japan.

2.2 Large laminar box for saturated sand

A laminar box should freely accommodate the movement of soil while neither resisting nor promoting soil movement. The design of the large laminar box involved identification and consideration of the issues important to the performance of the box. These included inertia, friction, membrane effects, boundary/corner effects (Prasad, et al. 2004), and consistency of the initial state of the volume of soil between tests. The inertia of a heavy container can alter the movement of soil within the container that the soil-container system no longer simulates the soil movements in free-field condition. To minimise this effect, the laminar layers should be of relatively low mass (Ueng, et al. 2005).

In view of this, a lightweight material had to be chosen for the laminar layers. To ensure that the box would not resist the movement of soil, a sliding system had to be developed to allow the layers to move with as little frictional resistance as possible. It had to be designed of sufficiently high flexibility to avoid any influence on the response of the soil, i.e. compliance effects (Prasad, et al. 2004).

Since the laminar box developed within this project will also be used to test saturated soils to study the effect of soil liquefaction, a waterproof membrane was used.

The boundary effects are typically localised along the edges of the box. At the centre of the soil mass, the effects are usually not significant. Thus, the laminar box was designed with a large surface area to ensure that a suitable volume of soil at and around the centre of the overall mass would remain relatively unaffected by boundary/corner effects. Other factors, such as the availability of materials, cost, ease of construction and repair, were also considered during the design process. Another important consideration was filling the box and saturating the sand in a reproducible manner.

Active earth pressures (Mononobe and Matsuo 1929, Matuo and Ohara 1976) were computed assuming that the entire box was filled with saturated soil. All components of the box were then designed to withstand the predicted loading. This box will be placed on a shake table and excited along its longitudinal axis. The final part of the design involved evaluating the structural integrity of all components of the box.

The laminar box has internal dimensions of 2 m × 2 m × 2 m. Each laminar layer can move horizontally, in the direction of the excitation, up to 175 mm. The soil inside the box can undergo a maximum shear strain of approximately 9%, which is enough to simulate the *in situ* epicentral displacement of soil under a large earthquake event. The box consists of three major components, that is, the base including barrier columns, the stack of laminar layers, and the membrane.

2.2.1 Base and Barriers

The details of the base are shown in Figure 2.1. The base has internal dimensions of 2 m × 2 m × 0.235 m and is made of 10 mm steel plate. Steel I-sections (200UB22.3) are welded horizontally on the transverse sides of the base. Three columns are welded onto the I-sections. These 2.45 m high 150UB14.0 columns also provide the main structural strength of the box. This height is selected for the preparation of the soil specimen (discussed in Section 2.2.4).

Rigid steel L sections brace the three columns (see red dashed line in Figure 2.1). These members minimise vibration of the columns in the longitudinal shaking direction. A row of M6 holes, at 53 mm c/c, is drilled on the flange of the columns that face the inside of the box. Each hole is used to fix a ball bearing for supporting a laminar layer. An 8 mm thick gusset is welded on the horizontal I-section directly under each column to facilitate load transfer to the base.



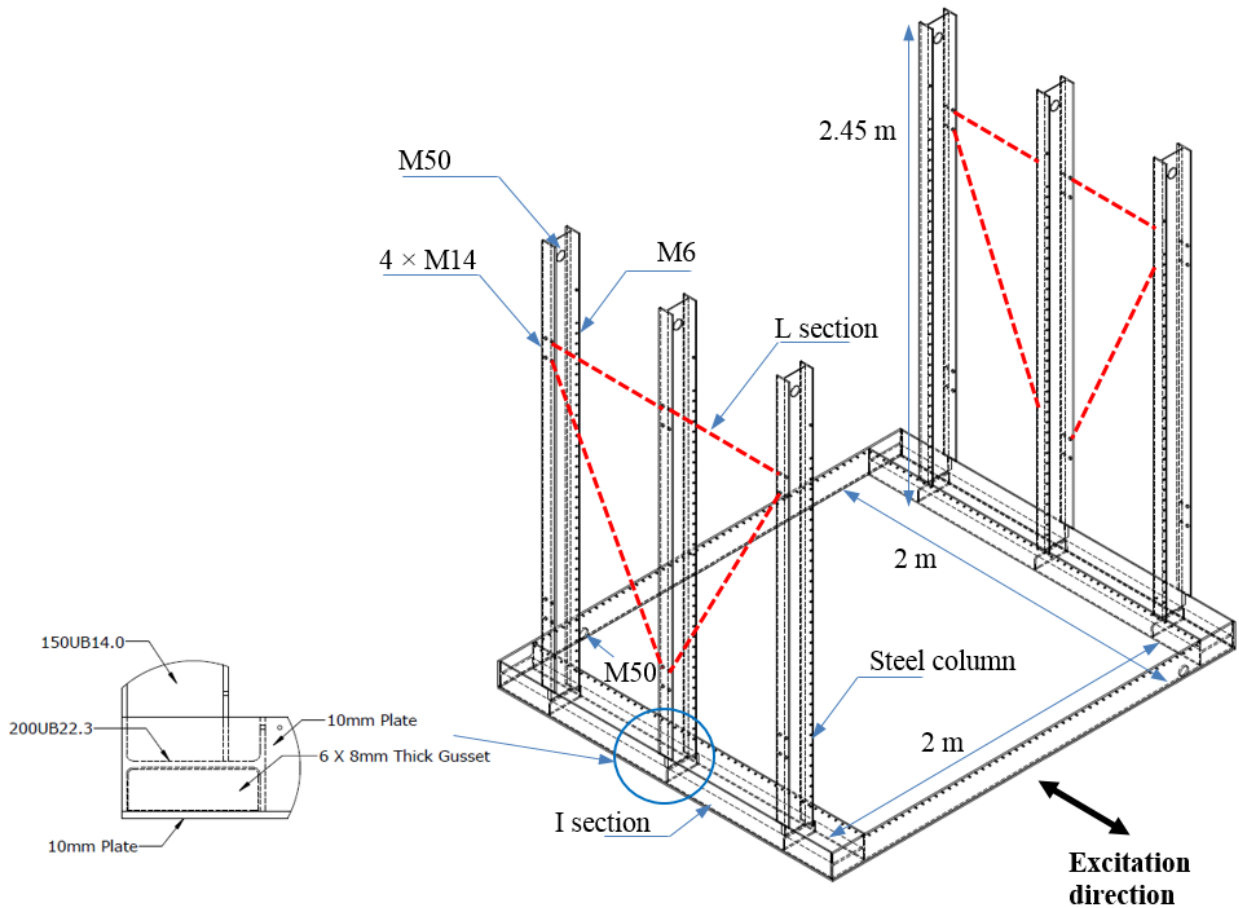


Figure 2.1. Details of the base and barrier columns

2.2.2 Laminar Layers

Thirty thin laminar layers (53 mm thickness) are used. Each of these layers is composed of a lightweight aluminium alloy that minimises the mass. Figure 2.2 shows the construction of the laminar layers. Each laminar layer is a frame made of a combination of x-shaped sections and 250 mm × 50 mm × 3 mm rectangular hollow sections. It was decided to use x-shaped sections as these sections have built-in tracks in which ball bearings are used to support the laminar layer. In this way, ball bearings are not installed between laminar layers, and the gap between the laminar layers is thus minimised. The x-shaped sections and rectangular hollow sections are bolted together using M12 bolts to form each layer.

Each layer is separated and supported by ball bearings fixed on the external columns. The ball bearings allow the layers to move relative to one other with little frictional resistance. A Teflon washer is provided between the x-shaped sections and the columns in order to reduce friction, thereby minimising resistance from the columns to the sliding of the laminar layers. As described in the previous section, the spacing between the holes for the ball bearings is 53 mm. The total thickness of the laminar layer is 50 mm (i.e., the height of the hollow section). Thus the gap between laminar layers is controlled to within 3 mm.

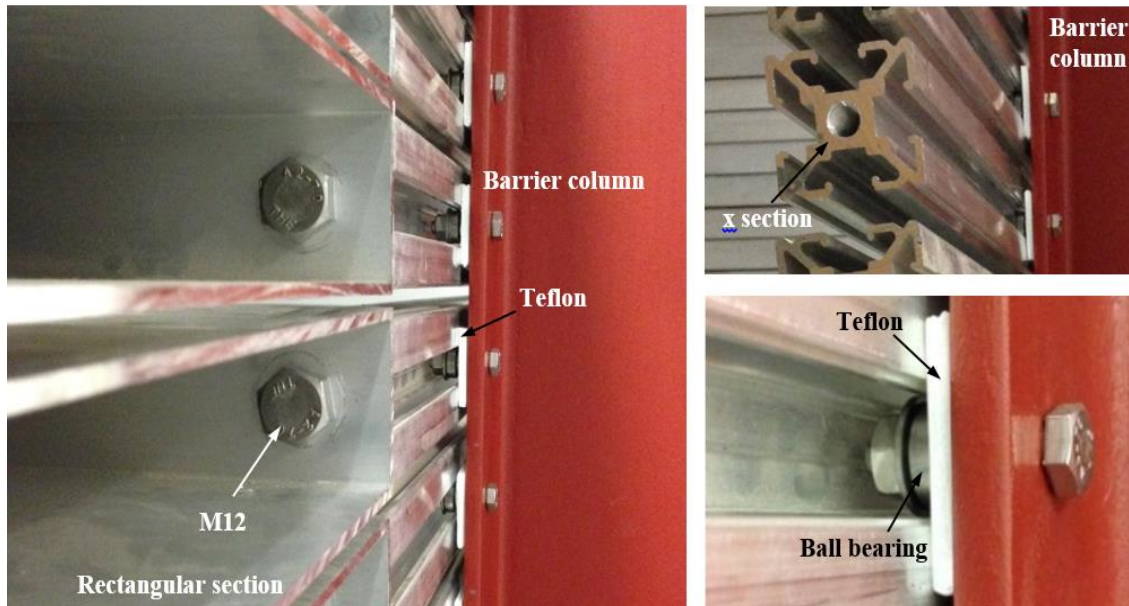


Figure 2.2. Construction of the laminar layers

2.2.3 Membrane

The third major component of the large laminar box is the membrane that lines the inside of the box. While most other laminar boxes, such as the one developed by Ueng et al. (2006), have utilised a silicone rubber membrane, the membrane in this box is made of a flexible and durable PVC fabric. It is chosen since it minimised the resistance to the movement of sand during shear. The fabric is designed to fold/unfold as sand moves against it rather than to stretch like a conventional silicone rubber membrane.

The membrane is made from a trapezium-shaped piece of fabric. The bottom of the trapezium has a length equal to the inner perimeter of the box, while the top of the trapezium is about 1.25 times longer than the bottom (Figure 2.3(a)). The bottom of the fabric is clamped to the steel base of the box, while the top of the fabric is pegged to the top laminar layer. The result is a fabric system that has increasing leeway with height above the base, reaching a maximum near the top of the box where the laminar layers are expected to move the most during testing (Figure 2.3(b)). This leeway allows the flexible membrane to fold/unfold easily to accommodate the movement of sand.

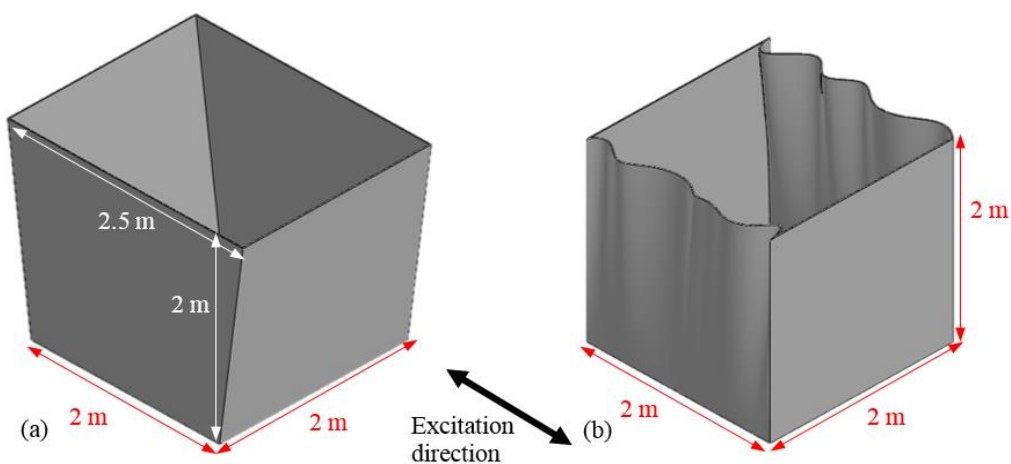


Figure 2.3. Size of the PVC fabric. (a) Prior to and (b) after fitting into the box



Figure 2.4. Top view of base and lateral membrane

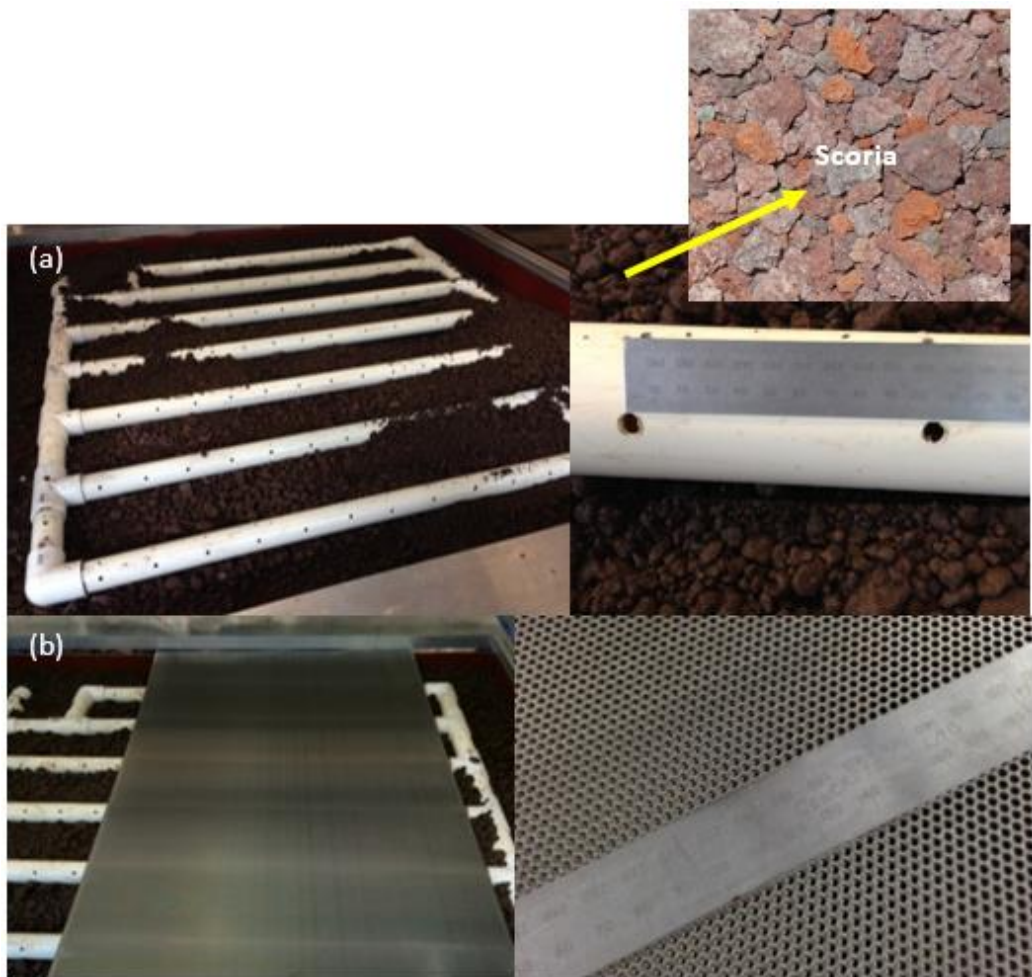


Figure 2.5. Construction of the base filter

At the base, two M50 holes allow the entry and exit of water. A piping system, with two rows of 8 mm holes, at 105 mm spacing, is connected to the inlet/outlet such that the water has a relatively uniform pressure distribution throughout the pipes (Figure 2.5(a)). There are a total of 180 holes in the pipe system.

The base also contains a filter layer (see Figure 2.5(b)), to prevent sand leaving the box, when water is released through the pipe system. The filter also assists in evenly distributing the water as it enters the sand in the box. The filter occupies the entire plan area of the cavity inside the base and is made out of separate layers (Figure 2.5(b)). The layers, listed in order from bottom to top are: metal perforated sheet, steel mesh, and another metal perforated sheet. The aperture size of the mesh is 0.04 mm, which is smaller than the minimum particle size of sand used in the study. The steel mesh prevents the sand from being drained out with the water. The perforated sheet is used to protect the steel mesh from damage, while at the same time allows the water to pass through. The pattern of holes of the perforated metal sheet is shown in Figure 2.5(b). This pattern is selected to minimise the size of the hole while maximising the opening area of the sheet. The diameter of the holes on the sheet is 2 mm. The perforated sheet has 40% of its area that is open.

2.2.4 Preparation of the sand specimen

In the case of tests on non-saturated sand, the laminar box was filled with 1 m depth of dry sand. This was achieved by raining the sand through a vertical distance higher than that required for the sand to reach terminal velocity (Figure 2.6). Raining of sand is a common technique that is used to prepare sand samples for laboratory testing (Ueng, et al. 2005, Qin, et al. 2013). A number of studies have been conducted to calibrate this technique (Vaid and Negussey 1984, Okamoto and Fityus 2006). It was reported that raining sand above the terminal falling height, determined to be above 400 mm, would allow for consistency in relative density over a wide plan area as the sand is deposited (Vaid and Negussey 1984, Rad and Tumay 1987).

In this study, a timber box with a base area of 2 m × 2 m was used to rain the sand. The base of the box was drilled with 1800 holes of 9 mm diameter with c/c spacing of 40 mm. This means that 2.8% of the area of the base consists of openings (Figure 2.6). During the raining process, the timber box was supported by the barrier columns of the laminar box. The maximum depth of sand in the laminar box is 2 m, and thus the clear distance between the base of the raining box and the maximum elevation of the sand surface is 450 mm. According to the data presented by both Rad and Tumay (1987) and Vaid and Negussey (1984), the relative density of the sand formed in the laminar box was about 35%. The sand properties achieved are listed in Table 2.1.

Figure 2.7 shows the pipe connection at the base of the laminar box for pumping the water into the pipe system (see Figure 2.5) for simulation of the behaviour of the saturated sand.



Figure 2.6. Test set-up. Laminar box with the raining box above

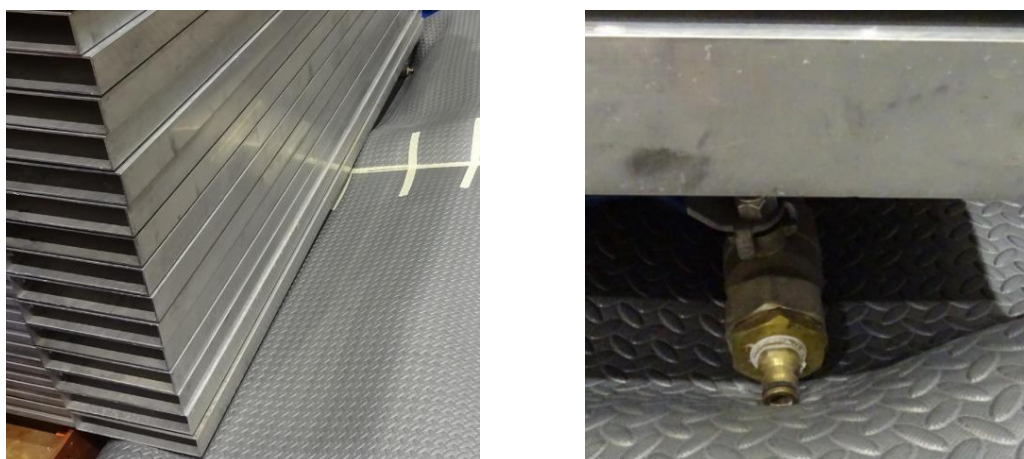


Figure 2.7. Water pipe connection

Table 2.1. Properties of sand used for dry tests

Density (ρ)	1451 kg/m ³
Unit weight (γ)	14.2 kN/m ³
Max. void ratio (e_{\max})	0.93
Min. void ratio (e_{\min})	0.60
Specific gravity (G_s)	2.67

2.3 General set-up of the large laminar box

Figure 2.8 shows the set-up of the experiments. To install the acceleration sensors within the sand three flexible plastic strips were hung vertically in the box to which three sub-surface accelerometers were attached. In addition, laser displacement transducers were installed to measure the displacement

of the sand surface along the centre line perpendicular to the axis of ground shaking. The acceleration of the sand surface was also measured. To have the actual data of the excitation, the table displacement (see Figure 2.9) was measured using a LVDT and the table acceleration with an accelerometer. The horizontal movements of three laminar layers were measured using laser displacement transducers.

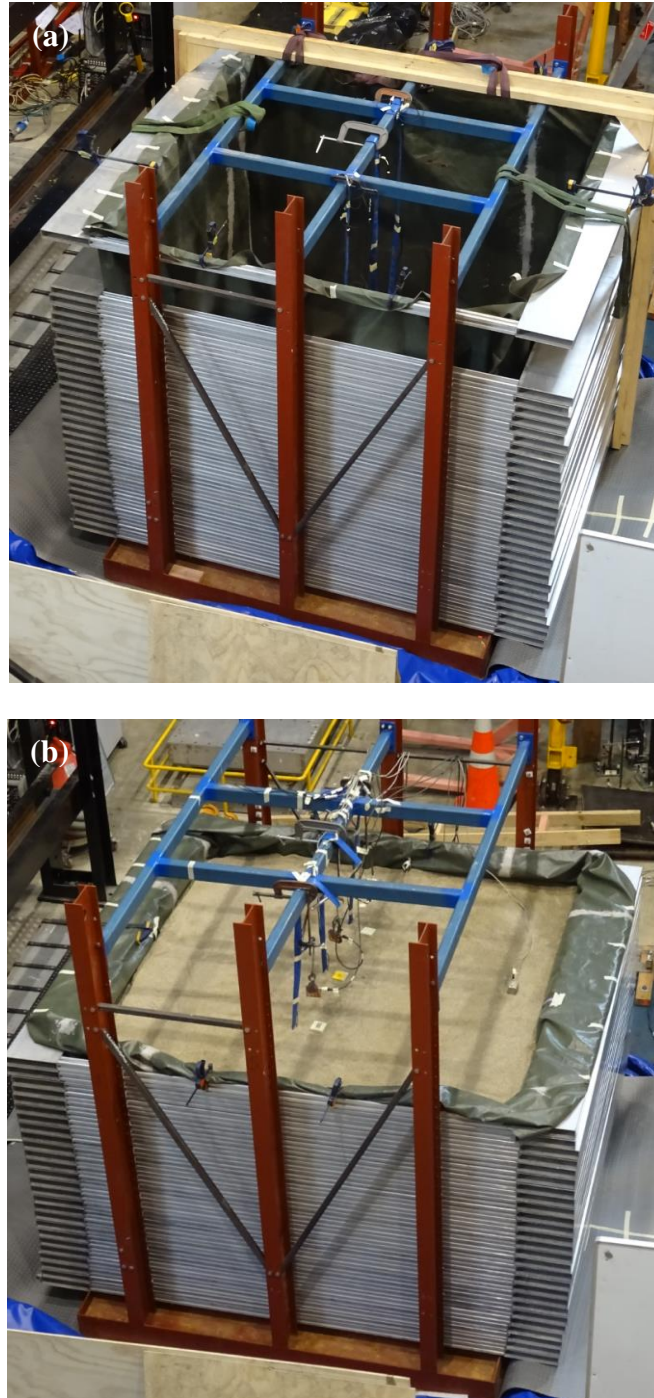


Figure 2.8. Laminar box. (a) Empty box (b) filled and instrumented box



Figure 2.9. LVDT and accelerometer at the table



Figure 2.10. Impact tests to obtain the shear wave velocity

To determine the shear wave velocity of the sand in the box a number of near vertical “down travelling SH wave” impact tests were performed, as shown in Figure 2.10. The development of the acceleration with the depth from the sand surface is shown Figure 2.11. The records from the accelerometer at 0.05, 0.7 and 1.35 m depth are presented in solid yellow, dashed red and dotted blue lines, respectively.

Since the distances between the sensors and the time the wave required to travel between sensors can be deduced, the shear wave velocity can be determined. The result was a value of SH wave velocity of approximately 144 m/s.

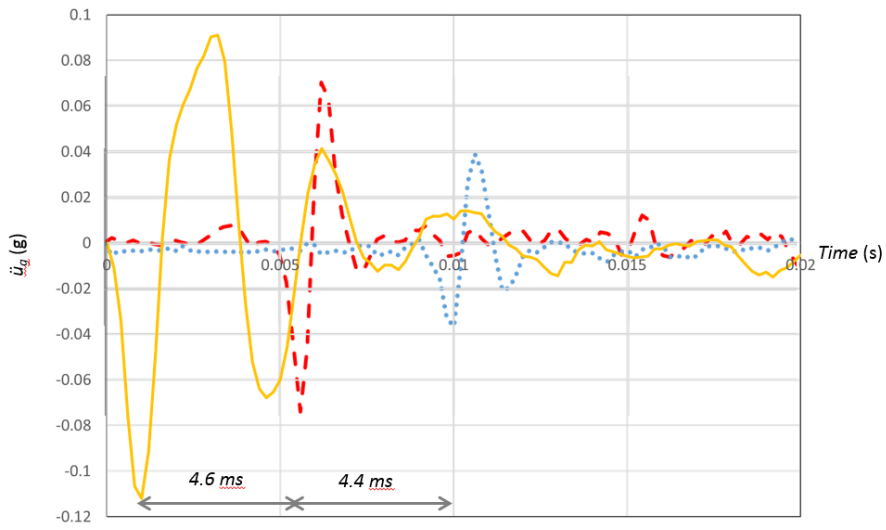


Figure 2.11. Effect of the depth location on the ground acceleration

3 INFLUENCE OF SOIL ON THE RESPONSE OF A SDOF STRUCTURE WITH A SHALLOW FOOTING

To investigate the influence of soil on the response of a single degree-of-freedom (SDOF) system the laminar box with 1 m depth of sand was placed on the shake table as shown in Figure 3.1. A frame model was placed on the sand surface. The model was assumed to be a SDOF model with a fixed base fundamental frequency of 2.8 Hz. The mass at the top was 19.2 kg and the height of the model was 580 mm. The footing size was 475 mm \times 475 mm. The footing was assumed to be rigid. Sand paper was attached under the footing to increase the friction at the footing-sand interface and thus minimise sliding.

The accelerations at the top (a_T) and at the footing (a_F) of the model were measured. The acceleration of the sand beneath the model (a_S) was measured by embedding another accelerometer in the sand directly beneath the centre of the footing of the model. Two laser transducers were used to measure the settlement at the sand surface and 250 mm away from the footing edge (Figure 3.1). The acceleration at the base of the laminar box (a_B) was also recorded. Strain gauges were attached to the base of the columns to measure the strain for calculating the bending moment development. The bending moments were used to calculate the base shears (V).

The excitation was simulated based on the Japanese design spectrum for a hard soil condition (JSCE 2000, Chouw and Hao 2005). Figure 3.2(a) shows the acceleration time history of the excitation. The peak ground acceleration (PGA) of the excitation is 0.79 g. The shake table used for this study was displacement-controlled with a maximum allowable movement of ± 120 mm. The displacement time histories of the excitations were obtained by double integration of the acceleration time history (Figure 3.2(c)). Because the maximum table displacement (335.57 mm) was larger than the allowable range of the shake table, it was decided to reduce the displacement of the excitation by a factor of four so that the maximum displacement of the ground motion is within the limit of the shake table. The ground acceleration is also reduced by a factor of four. This reduction led to a loading that is not strong enough to excite the structure. To keep the magnitude of the table acceleration correct (0.79g), according to Buckingham π theory (1914), the scale factor of the duration of the ground excitation needs to be two, because the scale factor of the table acceleration depends on the dimension of length and the dimension of time to a power of two. The relationship between the scale factors of length (S_L), time (S_T) and acceleration (S_a) is $S_T = \sqrt{S_L/S_a}$. To keep the acceleration magnitude correct the acceleration scale factor needs to be 1. Consequently, the scale factor for time is $\sqrt{4/1} = 2$. After scaling, the magnitude of the ground displacement is only 25% of the original magnitude (see Figure 3.2(d)), while the magnitude of the table acceleration time history has the same magnitude as the original acceleration (see Figure 3.2(b)). The duration of the table excitation is only 50% of the original duration (see Figure 3.2(b) and Figure 3.2(d)).

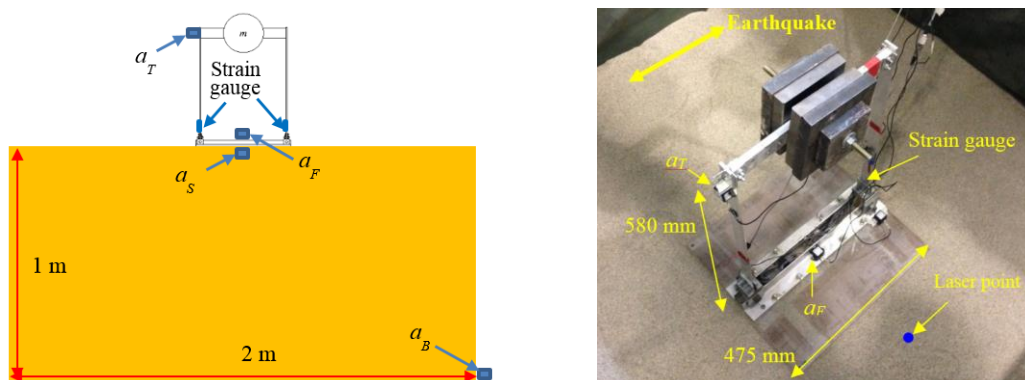


Figure 3.1. SDOF model with shallow footing

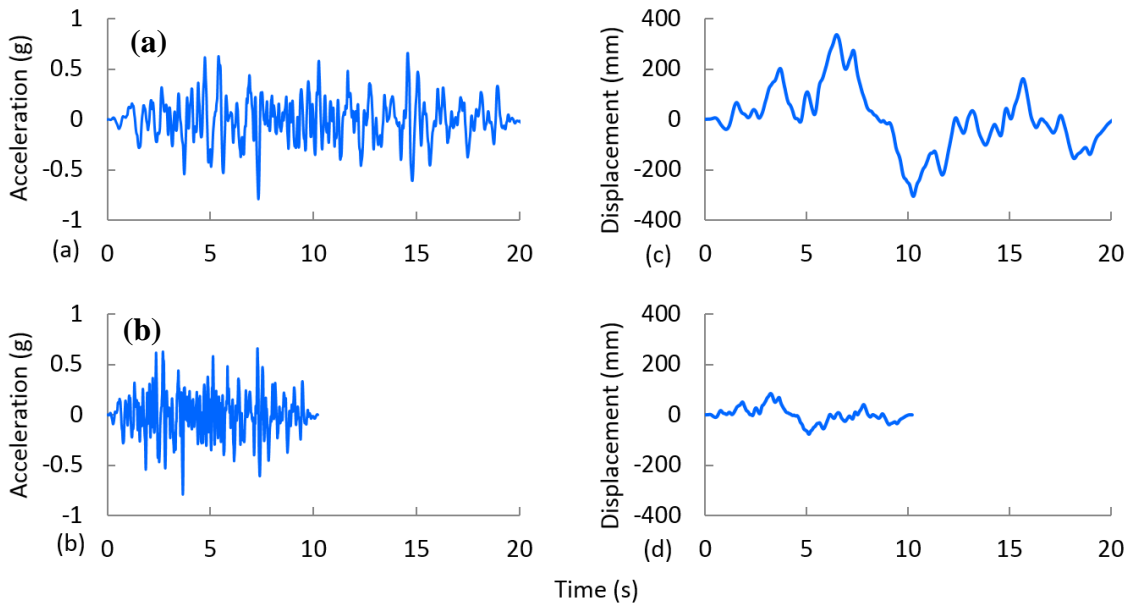


Figure 3.2. Scaled ground motion: (a) original table excitation (b) scaled table excitation as applied

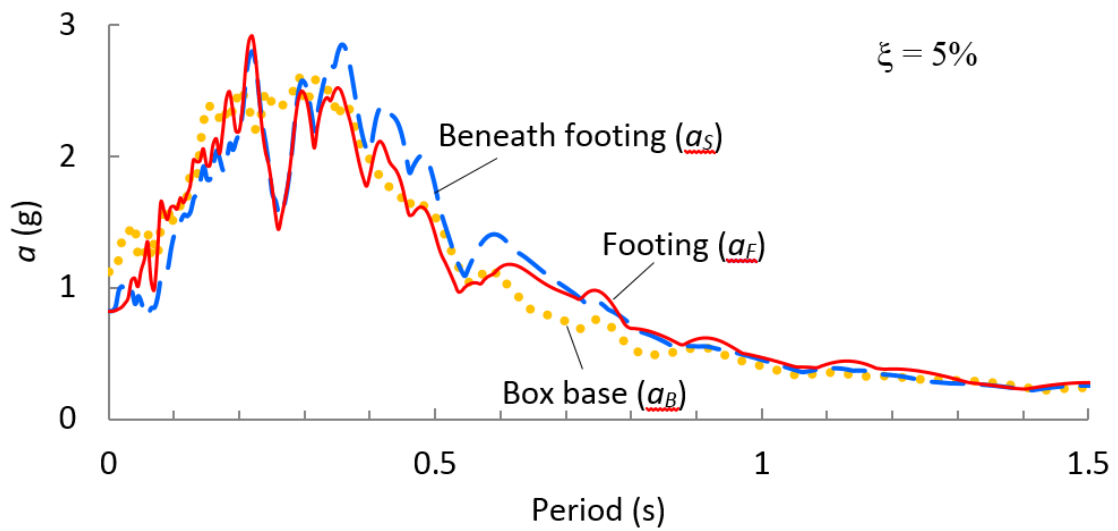


Figure 3.3. Response of SFS system

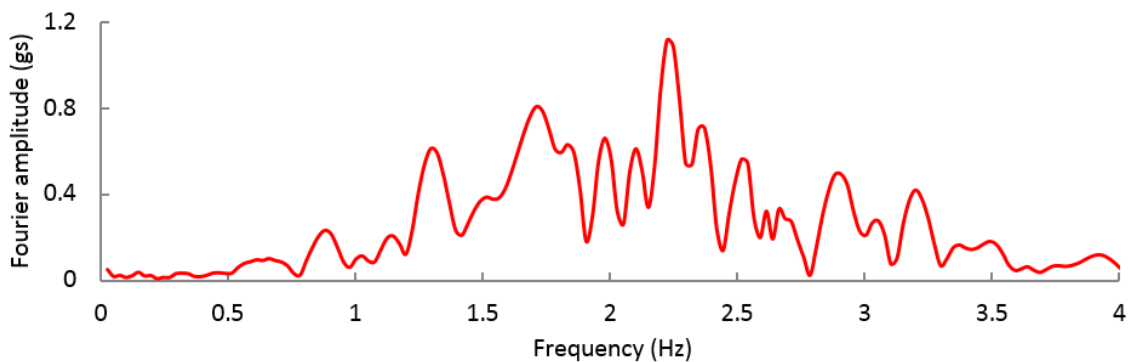


Figure 3.4. Frequency content of the acceleration at the top of the SDOF

Figure 3.3 shows the response spectra of acceleration at three different locations. The dotted line represents the response spectrum at the base of the laminar box (a_B). The dashed and solid lines are the response spectra of acceleration at the centre of the footing (a_F) and in the sand immediately beneath (a_S) the centre of the footing, respectively. In the mid to long period range (greater than 0.3 s), the spectral values of a_S are larger than those of a_B . In contrast, in the short period range (less than 0.2 s) the spectral values of a_S are lower than those of a_B .

Comparing the response spectra of acceleration at the footing (a_F) and under the footing (a_S), the spectral values of a_F are higher than those of a_S in the period range between 0.03 s and 0.2 s. In the long period range (greater than 0.7 s) the spectral values of a_F and a_S are similar. Other than that, the spectral values of a_F are lower than that of a_S .

The difference between the response spectra of a_F and a_S can be attributed to the interaction between the response of the model, the footing, and the soil. A part of the footing was observed to be temporarily separated from the supporting soil during all experiments. Because of the separation, the response spectrum of a_F around the fixed base fundamental period of the model (0.36 s) reduces.

Chopra and Yim (1985) developed an equation of motion to calculate the response of a structure with a flexible support. The deformation of the support was modelled using a two-spring support. They developed a set of formulas to calculate the maximum base shear (V_{max}) of structures on flexible supports:

$$V_{max} = V_{cr} \left\{ \frac{h^2}{R_o^2} + e^{-\xi\phi} \sqrt{\frac{b^4}{R_o^4} + \frac{b^2}{R_o^2} \left[\left(\frac{\check{S}_a}{g} \right)^2 \left(\frac{h}{b} \right)^2 e^{\xi\pi} - 1 \right]} \right\} \quad (3.1)$$

where:

$$\phi = \frac{\pi}{2} - \tan^{-1} \left\{ \frac{b}{R_o} \left[\left(\frac{\check{S}_a}{g} \right)^2 \left(\frac{h}{b} \right)^2 e^{\xi\pi} - 1 \right]^{-\frac{1}{2}} \right\} \quad (3.2)$$

and b is half of the base width and h is the height of the model; g is gravitational acceleration; $R_o = \sqrt{h^2 + b^2}$ (diagonal distance from the mass to an edge of the footing) and $V_{cr} = mg \times b/h$ is the base shear to initiate footing uplift. \check{S}_a is the spectral acceleration corresponding to the effective vibration period \check{T} . The effective vibration period of a structure with a flexible support is:

$$\check{T} = T \sqrt{1 + \frac{k_h}{k_\theta}} \quad (3.3)$$

where T is the fundamental period of the structure with a fixed base, k_h is the lateral bending stiffness of the structure and k_θ is the rotational stiffness, assumed to be the static stiffness, of the footing on uniform soil:

$$k_\theta = \frac{G\pi}{8(1-\nu)} B^2 \quad (3.4)$$

where G and ν are the shear modulus and the Poisson's ratio of the soil, respectively. B is the base width ($=2b$).

An empirical equation was developed by Larkin (1978a) such that the shear wave velocity (V_s) of sand can be calculated using the relative density (D_r), mass density (ρ) and mean effective confining stress (σ'_M):

$$V_s = \sqrt{\frac{D_r + 25}{100}} \times \left[\sqrt{\frac{0.422 \times 10^6}{\rho}} \sqrt{\sigma'_M} \right] \quad (3.5)$$

The shear wave velocity can be used to calculate the shear modulus of soil:

$$G = \rho V_s^2 \quad (3.6)$$

By combining Equations (3.5) and (3.6), Equation (3.7) can be obtained to estimate the shear modulus (G) of sand using the relative density D_r and effective confining stress σ'_M .

$$G = \frac{D_r + 25}{100} \times \sqrt{0.422} \times 10^3 \times \sigma'_M \quad (3.7)$$

The shear modulus of the sand at a depth of 59 mm is thus 0.45 MPa. This depth, calculated from 1/8th of the footing width, is the appropriate depth for a characteristic soil element to represent the stress conditions of soil involved in providing resistance to moment and shear (T. Larkin 2008). The effective vibration frequency of the model on sand, using this calculated shear stiffness and Equations (3.3) and (3.4), is 2.74 Hz. The effective vibration period of the model is very similar to the fixed base fundamental period. This is because in shake table experiments (1g conditions) the sand cannot be scaled. As a consequent of this, the sand has a larger stiffness than that of a scaled sand. Consequently, the unscaled sand has a higher shear modulus, i.e. higher sand stiffness.

Figure 3.5 shows a comparison of the maximum base shear (V_{max}) of the model obtained using experimental data and Equation (3.1). Strain gauge measurements are used to determine the maximum bending moment at the base of the model, and thus the experimental maximum base shear can be calculated. The spectral acceleration $\check{S}_a(\check{T})$ is derived from the acceleration measured in the soil beneath the footing (Figure 3.3). It can be seen that Equation (3.1) overestimates the maximum base shear of the model. The experimentally obtained maximum base shear for the model is 169.5 N. With Equation (3.1), the corresponding maximum base shears are 249.4 N. Equation (3.1) overestimates the maximum base shear of model by 47%.

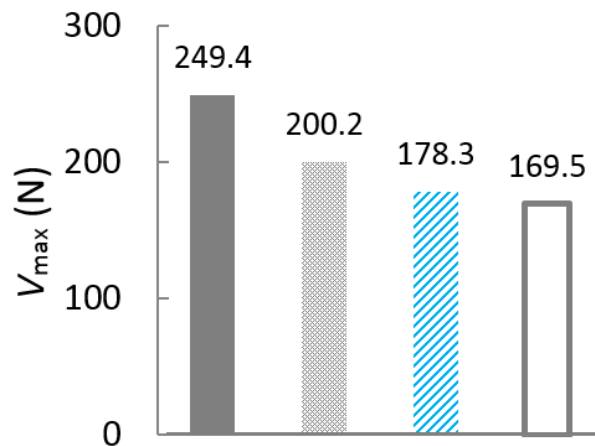


Figure 3.5. Maximum base shear from analytical calculations and experiment

The accuracy of Equation (3.1) is associated with the estimation of the effective vibration period of the model on sand. In Equation (3.3), the rotational stiffness of the footing on soil is modelled using elastic springs. Footing uplift and soil plastic deformation are not considered. Therefore, the effective vibrational period of the model is underestimated.

As shown in Figure 3.4, the maximum Fourier amplitude of the top of the structure is found at 2.22 Hz. This indicates that the corresponding vibration period (\tilde{T}) is 0.45 s, hereafter denoted as \tilde{T}_f . Compared with the theoretical calculation ($\tilde{T} = 0.36$ s), Equation (3.3) underestimates the effective vibration period by 20%. When \tilde{T}_f is used to obtain the spectral value, the accuracy of Equation (3.1) can be improved. The maximum base shear of the model, estimated using $\check{S}_a(\tilde{T}_f)$, is 200.2 N. Although Equation (3.1) overestimates the maximum base shears by 18%, the calculations are closer to the experimental results. To further improve the accuracy of Equation (3.1), the spectrum acceleration derived using footing acceleration (a_f) in conjunction with \tilde{T}_f can be used. The maximum base shear obtained from Equation (3.1) using $\check{S}_a(\tilde{T}_f)$ is 178.3 N. The error reduces to 5%.

The results show that when comparing experimental results against those from an existing theoretical method, the accuracy of the method is sensitive to the effective vibration period of the SFSI system and the spectrum acceleration of the footing.

4 SUBSURFACE BEHAVIOUR OF SATURATED SAND AND THE EFFECTS OF SHALLOW FOOTINGS

4.1 Introduction

The importance of liquefaction was brought into stark relief by the Canterbury series of earthquakes which inflicted considerable liquefaction-induced damage on the city of Christchurch. The visible effects of liquefaction are mainly associated with settlement and rotation of structures, rupture and uplift of underground services and deformation damage of roads. This report presents the results and interpretation of a series of liquefaction tests using the laminar box on a shake table. The work investigates excess pore pressures, accelerations and lateral displacements under harmonic and earthquake loading in the soil surrounding model footings as well as the free field.

Parameters, such as the acceleration of the structure, are commonly assumed in codes to be either not modified or reduced compared to the non-liquefaction situation. Additionally, even in the presence of structures, design codes worldwide commonly consider only the soil characteristics and the strength and duration of ground shaking to evaluate the liquefaction hazard. Examples of the current industry approaches to study the liquefaction potential are the Guidelines presented by the Ministry of Business, Innovation and Employment in New Zealand (MBIE 2016) and the works by Youd et al. (2001), Seed, et al (2003) and (Idriss and Boulanger 2008) in the US.

One of the principal aims of this work is to reveal how the presence of structures affects the soil-footing system response by developing an understanding of the development and dissipation of excess pore-water pressure in the presence of footings. This work considers footings only (i.e. no superstructure) in an effort to diminish the complexities and enable an understanding of the response of the soil-footing system using a holistic approach considering the generation and dissipation of excess pore-water pressure.

Most recorded cases of liquefaction have been found to occur at relatively shallow depths, i.e. less than 10 m below the ground surface. Although even in the presence of sand boils it is not always clear where the liquefaction initiated. To gain an understanding of the process of liquefaction, laminar box tests were carried out and recording of ground response at depths of 0.05, 0.7 and 1.35 m were obtained. The intent in this report is to present that information as well as derive an understanding of the process leading towards liquefaction, or in some cases, development of significant excess pore-water pressure without liquefaction. Carrying out dynamic tests in the low effective stress regime brings experimental difficulties due to low signal strength leading to poor signal/noise ratios and potential loss of linearity in the instruments, as well as the inherent confining pressure-dependency of soil properties.

The 2×2 m laminar box (Figure 4.1) described in Section 2 was used primarily because it is a consistent domain where free-field response and soil-structure interaction can be investigated in a holistic manner. The laminar box has been designed to reproduce the deformation state of the sand during the passage of seismic waves, which are assumed to propagate vertically from a hard medium to the ground surface (i.e. SH waves). Thus, the state of deformation of the sand and the boundary conditions are reasonably consistent with 1D seismic ground response (X. Qin 2016).

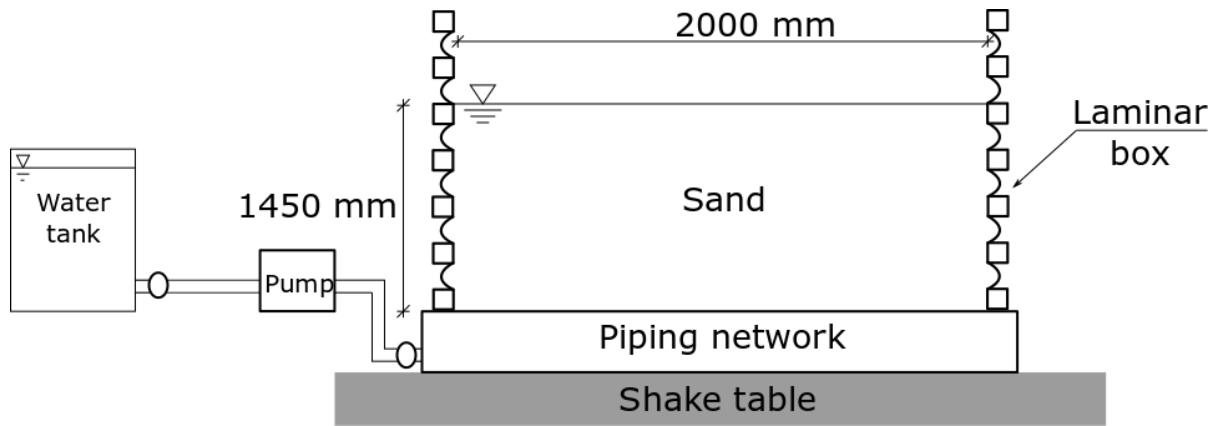


Figure 4.1. Schematic sketch of test rig

4.2 Methodology

The scaling laws associated with physical testing (Buckingham Theory) were not applied in the case of these experiments. Thus all measurements were unscaled and therefore only apply to these experiments which were carried out in a 1g environment, i.e. the results are presented in model scale. An approximation in the experiments is the contact stress of the footings is not sufficient to provide a pressure similar to that of a typical building. However the size of the model is large enough that the deductions from the measurements are meaningful. An advantage of not having the necessity of using scaling laws is that water may be used in the void space ensuring that the correct dissipation rate of excess pore pressure is maintained, i.e. the scaling factor for water viscosity and density is 1.

All the tests were performed using the 2×2 m laminar box filled with a quartz sand taken from the Waikato River. After the initial filling of the box, several episodes of shaking, using white noise with a frequency content from 1 to 10 Hz, were applied until a constant height was achieved (i.e. no further surface settlement was recorded). A final height of 1.45 m was obtained, with relative density of 51%.

The laminar box system was designed with a piping network beneath the sand, including a pump to flush water from the base to the surface of the sand. The piping network beneath the sand has holes spaced at 100 mm intervals that allow entry of the water into the mass of sand (Figure 4.2). This piping network is half-buried in a coarse granular material to distribute the load of the soil and is covered by a fine mesh to avoid sand clogging the holes. For further details of the laminar box design and operation, refer to Section 2 above and Qin (2016).



Figure 4.2. Pipe system at the base of the laminar box

The flushing of water through the sand caused sand boils over the majority of the surface of sand leading to a relatively consistent density across the soil volume. Following this, the water was drained from the sand and successive cycles of wetting and draining performed. This process was followed prior to all imposed shaking of the box to reset the initial conditions of the soil. The entire process (emptying and refilling) takes approximately two hours. The final height of the sand was measured after draining excess water until the water table was just below the surface of the sand. The final thickness of the sand had a variability of ± 2 mm across all the tests. The height of the water table was measured using a transparent hose attached to the outside of the base of the laminar box.

4.2.1 Soil properties

Waikato river sand was used in these tests. This sand is a clean, poorly-graded quartz sand with angular particles, with a small percentage of particles of volcanic origin. The properties of the soil are presented in Table 4.1.

Table 4.1. Properties of the soil used in saturated tests

	Parameter	Value	Unit
At the time of the tests	Dry density	1571	Kg/m ³
	Void ratio	0.66	
	Relative density	51	%
	Permeability*	2.21×10^{-3}	cm/s
General properties	Specific gravity	2.64	
	Minimum void ratio	0.55	
	Maximum void ratio	0.78	
	D50	0.82	mm
	D10	0.47	mm

* Estimated from Hazen's (1930) equation for clean filter sand assuming $c = 1.0$

The particle size distribution of the sand is presented in Figure 4.3. The liquefaction limit curves proposed by the Technical Standards for Port and Harbour Facilities in Japan (2009) are also presented as a reference. The particle size distribution of the sand employed is at the extreme right-hand limit of the high liquefaction risk region. In a general sense this would imply that, based on PSD only, the behaviour of the sand will lie somewhere between a very rapid pore-water pressure response and a gradual accumulation of excess pore-water pressure.

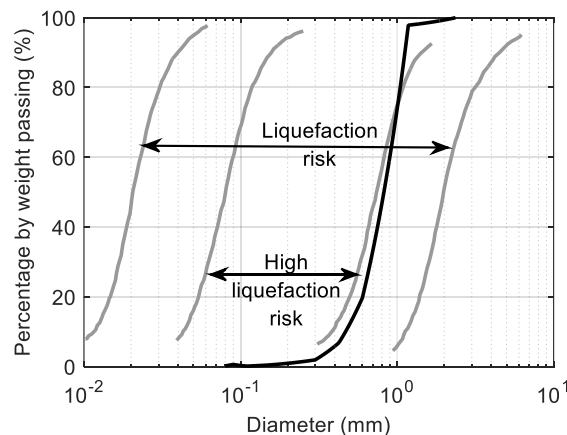


Figure 4.3. Particle size distribution

4.2.2 Instrumentation

The acceleration was measured in the soil at depths of 0.05, 0.7 and 1.35 m (Figure 4.4-a). The pore-water pressure was also measured at the same depths but offset by 0.15 m from the accelerometer array. Laser displacement transducers were used to measure the lateral displacement of the laminar layers of the box at points 0.05, 0.20 and 0.40 m beneath the level of the surface of the sand. The acceleration on top and the vertical deformation of the footings were measured (Figure 4.4-b). The vertical deformation was measured using LVDTs close to the edges of the footing. The settlement at any given time is obtained as the average of both LVDTs.

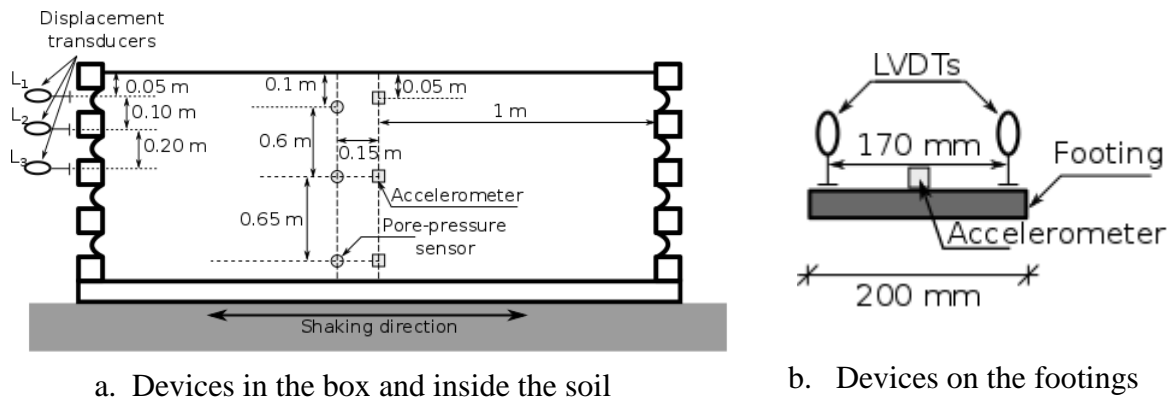


Figure 4.4. Schematic elevation showing the location of the instrumentation (Not to scale)

4.2.3 Footing models

Rigid steel blocks were used to model the footings. The rigid material was used to avoid any deformation of the footings. All blocks had the same dimensions and weight. The plan dimensions were 0.2×0.2 m and 0.025 m height (see Figure 4.5). These dimensions ensured that the distance between the edge of the footings and the closest edge of the soil container was larger than three times the footing width (thus boundary effects are negligible). The footings dimensions also need to be sufficient to reflect the potential for variation in excess pore-water pressure across the length of the footing. The mass of each footing was 77 N (assuming a uniform bearing pressure yields 1.93 kPa). Sandpaper was glued to the base of the footings to simulate the friction between a concrete footing and the sand.

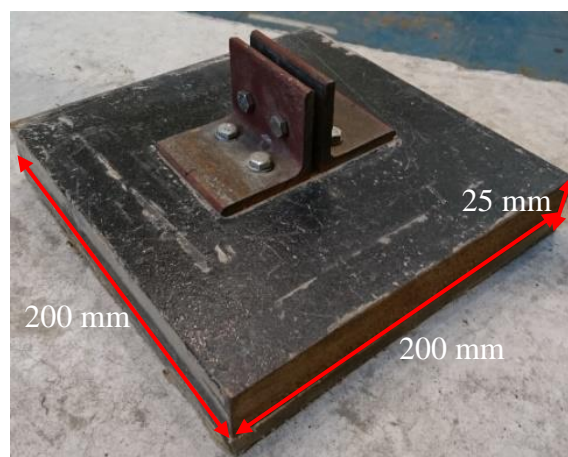


Figure 4.5. Footing model

4.2.4 Tests configurations

The free-field condition (no footings) was initially subjected to a range of ramped harmonic loads and a recorded earthquake ground motion. Two configurations of surface footings were also studied to investigate the effects of clustering of the footings under these loadings. The configurations of the footings were:

1. A stand-alone footing, at the centre of the laminar box.
2. A cluster of six footings (two rows of three footings in the direction of the shaking).

A distance of $B/4$ between all footings was maintained. A schematic of the plan view of these configurations is presented in Figure 4.6.

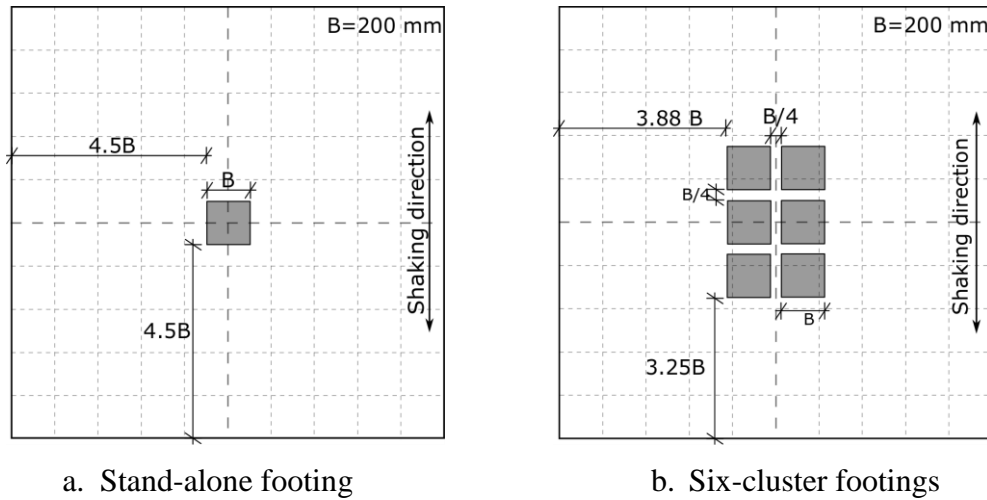


Figure 4.6. Plan view of the footing configurations

4.2.5 Ground motions

Ramped harmonic waves, utilising four cycles to achieve (and decrease from) the maximum acceleration, were used. For the free-field tests, 20 cycles of steady-state motion (constant acceleration amplitude) were applied. A maximum acceleration of 0.20 g was applied. Frequencies of 1, 1.5 and 2 Hz were utilised in these tests (Table 4.2). A recorded ground motion from the Darfield earthquake was also utilised (Table 4.3).

Table 4.2. Properties of the harmonic motion

Property	Value
Frequency (Hz)	1, 1.5 and 2
Maximum table displacement (mm)	50 (1 Hz) , 22 (1.5 Hz) and 12.5 (2 Hz)
Maximum acceleration (g)	0.20
Number of steady-state cycles	20

Table 4.3. Properties of the recorded ground motions

Ground motion	Magnitude	Station	Maximum acceleration (g)
Darfield earthquake (04/09/2011)	7.1 (M_w)	RKAC	0.21

As shown in Table 4.2, the table displacement is inversely proportional to the square of the frequency. This has a very important effect, e.g. the 2 Hz motion induces a displacement of 25% of the 1 Hz motion. However, the shear deformation is not only controlled by the displacement of the table, but also by the response of the soil as a free body, which is a function of the frequency and acceleration.

4.3 Results and discussion

The boundary conditions in a shake table experiment are different from the often performed cyclic undrained triaxial test (often known as a liquefaction test), where the specimen is constrained by a zero volume change condition. In the case of shake table testing there is a free surface and hence the sand can undergo volumetric strain and drainage of excess pore pressure. Volume change (dilation), and hence drainage, is more likely to occur in the near surface zone where effective stress is low.

One of the most important parameters to be evaluated with respect to earthquake loading of saturated cohesionless soils is the excess pore-pressure. In the case of most laboratory tests, the excess pore pressure will be a monotonically increasing quantity with time; this view is often created by reviewing laboratory test results where the tests are carried out under undrained (constant volume) conditions. However, this may not be true for *in situ* conditions where drainage, at times of a low rate of pore pressure generation, will lead to periods of net pressure loss, especially for near surface zones.

In addition, in zones of low effective stress there is a tendency for dilation to occur at times of large shear strain. This increase in volume will affect the permeability and lead to changes in permeability and hence drainage, as was discussed by Hyodo, et al (2002). Analytically what is required is the coupled solution of the wave equation and the equation for dissipation with a source pore water pressure term include Larkin (1978b).

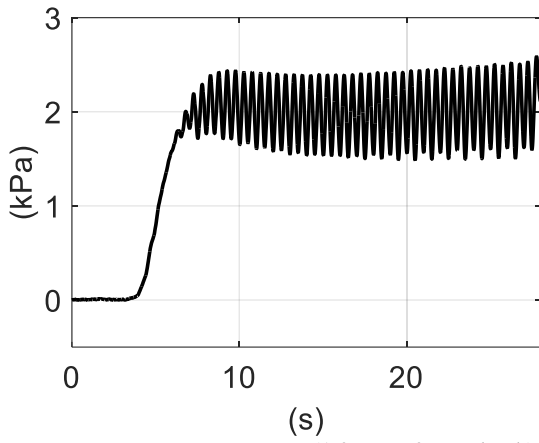
Co-excitation redistribution and dissipation at the free surface of excess pore pressure will take place in the sand according to the instantaneous gradients of total head in time and space and the permeability of the sand. Thus the recorded excess pore pressure at any point is affected by the response of the whole body of sand. The contents of the laminar box should be regarded as a “system”, responding to excitation by generating point-wise excess pore pressure under the boundary conditions prevailing, including a transient (non-steady) flow regime. There will be gradients in the vertical and horizontal directions, creating a complex 3D flow field. The records of excess pore pressure presented in this report are the combination of the generation and concurrent dissipation (redistribution) of excess pore pressure. It is not possible to quantitatively separate these two features in the data presented.

4.3.1 Free-field

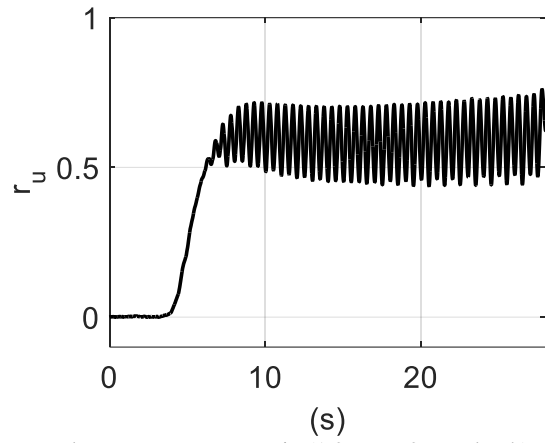
Harmonic loads

The pore-pressure evolutions for the harmonic base motions at 0.7 m depth are presented in Figure 4.7 to Figure 4.9, while those at 1.35 m depth in Figure 4.10 to Figure 4.12. All these figures also present the pore-pressure ratio as an indication of how close the soil is to a fully liquefied condition. The pore-pressure ratio (r_u) at a sub-surface point, as defined in Equation (4.1) corresponds to the ratio of the excess pore-water pressure (u_{ex}) to the initial vertical effective stress at the same depth (σ'_{vo}). Therefore, a value of $r_u = 1$ corresponds to a fully liquefied state.

$$r_u = \frac{u_{ex}}{\sigma'_{vo}} \quad (4.1)$$

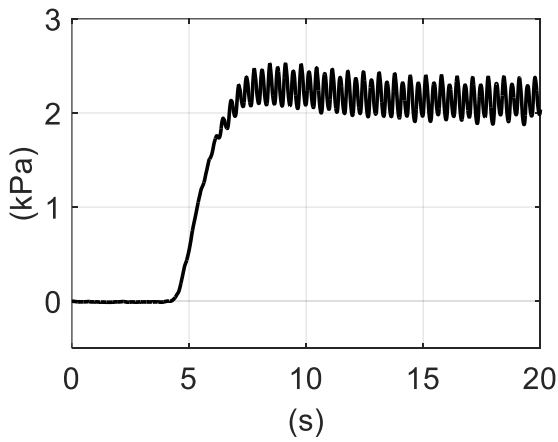


a. Excess pore-pressure (1.0 Hz at 0.7 m depth)

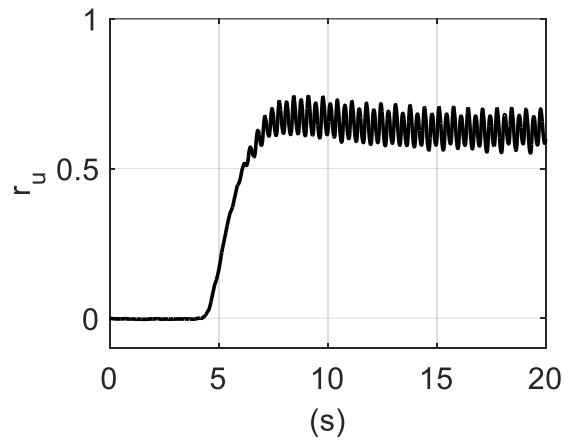


b. Pore-pressure ratio (1.0 Hz at 0.7 m depth)

Figure 4.7. Excess pore-pressure and pore-pressure ratio (free-field - 0.7 m depth - 1 Hz)

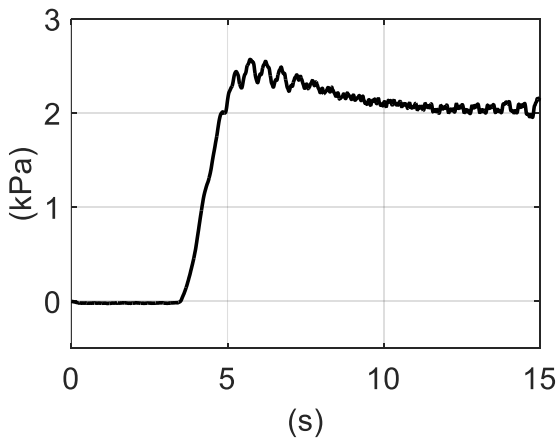


a. Excess pore-pressure (1.5 Hz at 0.7 m depth)

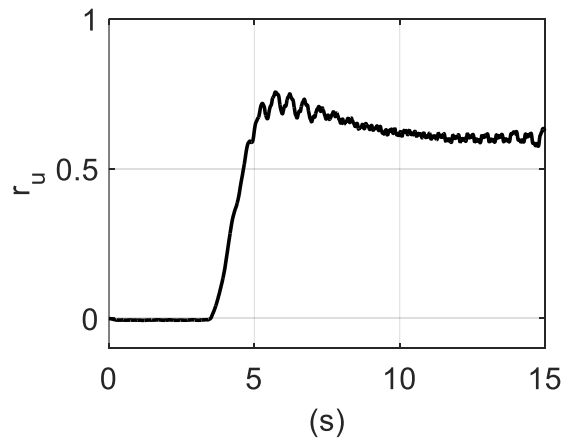


b. Pore-pressure ratio (1.5 Hz at 0.7 m depth)

Figure 4.8. Excess pore-pressure and pore-pressure ratio (free-field - 0.7 m depth - 1.5 Hz)

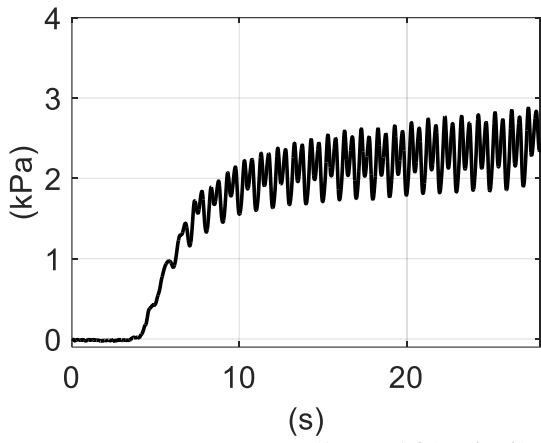


a. Excess pore-pressure (2 Hz at 0.7 m depth)

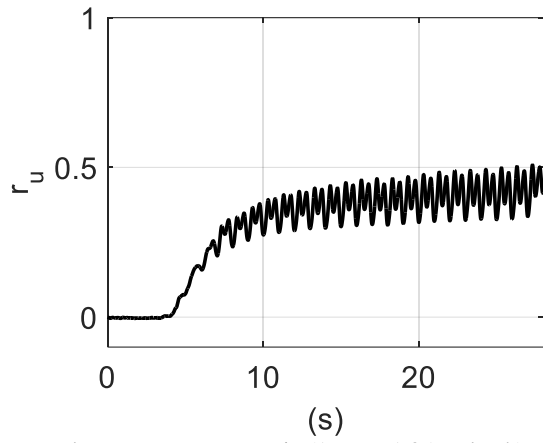


b. Pore-pressure ratio (2 Hz at 0.7 m depth)

Figure 4.9. Excess pore-pressure and pore-pressure ratio (free-field - 0.7 m depth - 2 Hz)

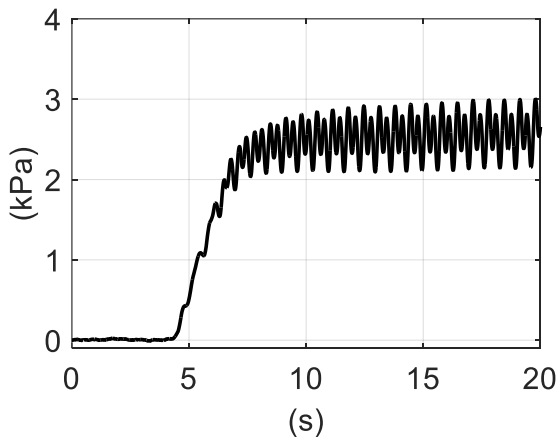


a. Excess pore-pressure (1 Hz at 1.35 m depth)

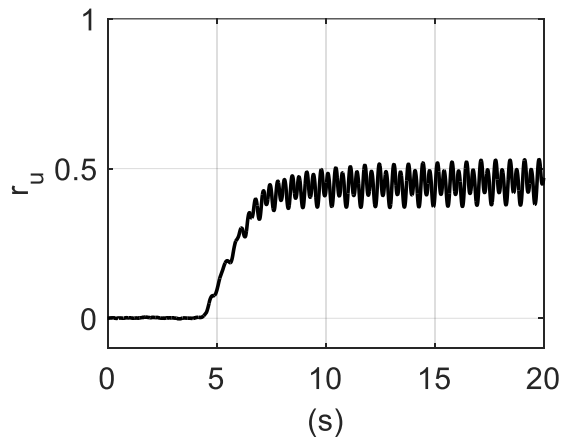


b. Pore-pressure ratio (1 Hz at 1.35 m depth)

Figure 4.10. Excess pore-pressure and pore-pressure ratio (free-field - 1.35 m depth - 1 Hz)

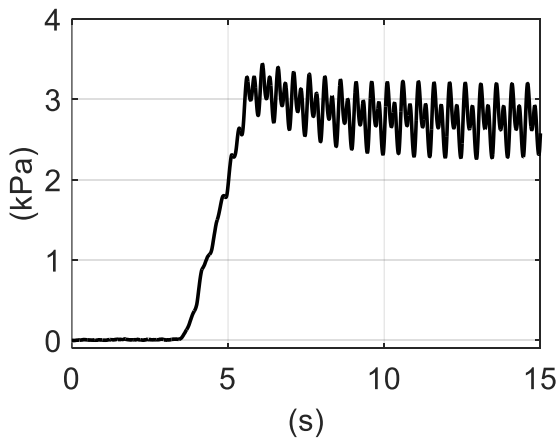


a. Excess pore-pressure (1.5 Hz at 1.35 m depth)

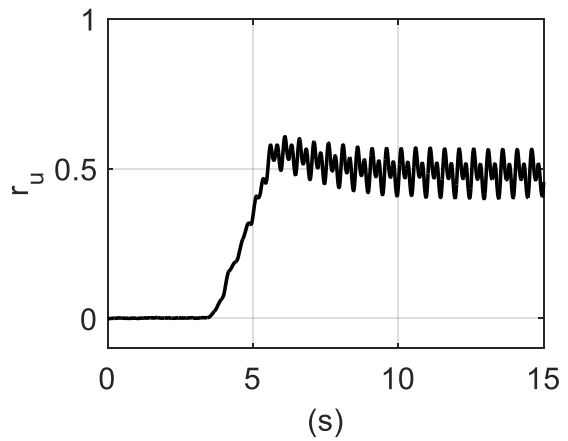


b. Pore-pressure ratio (1.5 Hz at 1.35 m depth)

Figure 4.11. Excess pore-pressure and pore-pressure ratio (free-field - 1.35 m depth - 1.5 Hz)



a. Excess pore-pressure (2 Hz at 1.35 m depth)



b. Pore-pressure ratio (2 Hz at 1.35 m depth)

Figure 4.12. Excess pore-pressure and pore-pressure ratio (free-field - 1.35 m depth - 2 Hz)

The following major points may be noted in the sand response across the 3 frequencies and depths:

1. As the frequency increases the amplitude of the oscillatory motion reduces. This is thought to be due to a reduction in rate of drainage compared with the rate of generation of pore pressure.
2. The oscillatory part of the pore pressure response occurs in the region of high pore pressure where the shear deformation is large and the effective stress is low.
3. At 0.7 m depth there is little variation in the peak pore pressure with frequency, while at 1.35 m the peak pore pressure increases with frequency.
4. For both depths, 0.7 m and 1.35 m the maximum r_u value hovers about 0.5 for all frequencies
5. At a depth of 0.7 m the pore pressure response to a 2 Hz excitation is of a different nature to the other records. The cyclic fluctuations, while being present, are much suppressed.

Figure 4.13 below shows a time-window of the excess pore-pressure (u_{ex}) and the corresponding displacement of the shake table. A significant cyclic component is evident in many cases, generated by cyclic shear stress reversal, with the pore-pressure increases independently of the sign of the shear stress every half cycle. This leads to the cyclic component of excess pore pressure having a frequency approximately twice that of the shake table, but approximately in phase. Also evident is a monotonically increasing component, defined as the excess pore pressure at zero table displacement, which may be seen as the black curve approaches the grey curve (which has a constant amplitude). A small increase in excess pore pressure over the 2 seconds of the record is evident in the monotonic component.

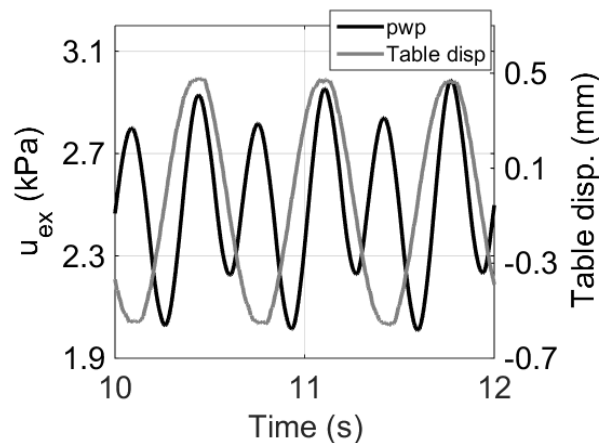
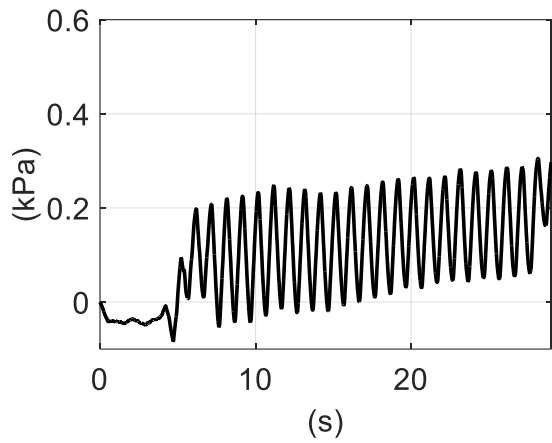
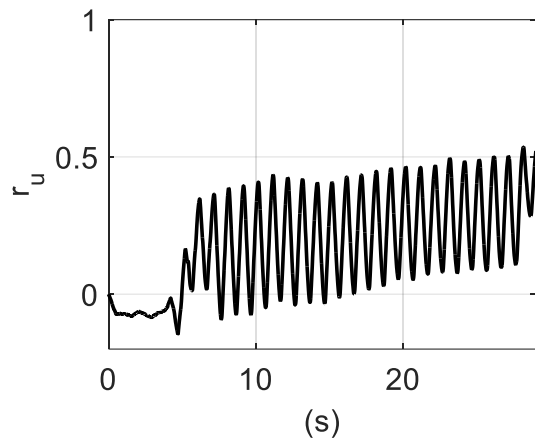


Figure 4.13. Oscillating behaviour at 1.35 m depth and a frequency of 1.5 Hz

The dynamic pore-pressure recorded by the shallowest device (0.1 m) is presented in Figure 4.14 to Figure 4.16 for the 3 frequencies 1, 1.5 and 2 Hz. The response at this depth is of a different nature to the deeper records of pore pressure, but does have a cyclic component for the 2 lowest frequencies. The nature of the response to the 2 Hz excitation is different from the other 2 frequencies. The cyclic component is much diminished and there is a rapid drop in pressure following the peak response. In this near surface zone, with a closely adjacent free surface and therefore very low effective stress, there is likely to be dilative and very rapid drainage effects leading to significant changes in the pore pressure, compared to material at depth. In this zone the structure of the soil is likely to be grossly disturbed and possibly defined drainage channels formed.

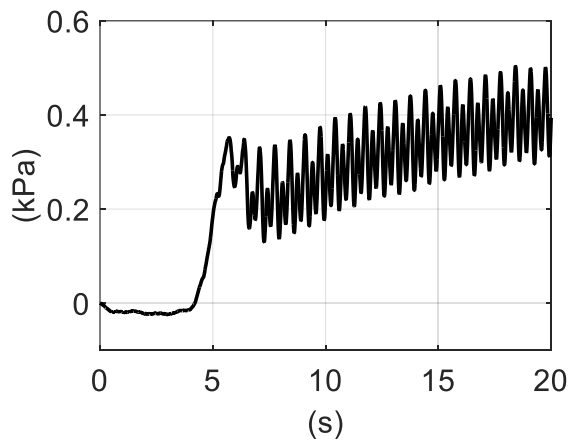


a. Excess pore-pressure

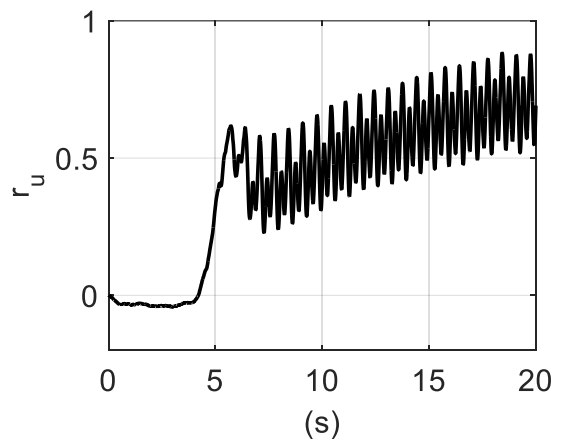


b. Pore-pressure ratio

Figure 4.14. Excess pore-pressure and pore-pressure ratio at 0.1 m depth (free-field - 1 Hz)

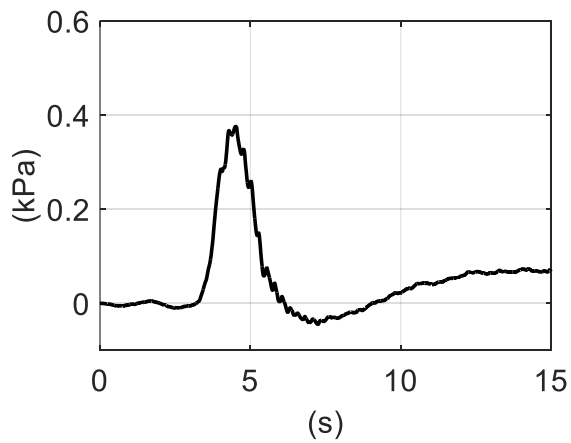


a. Excess pore-pressure

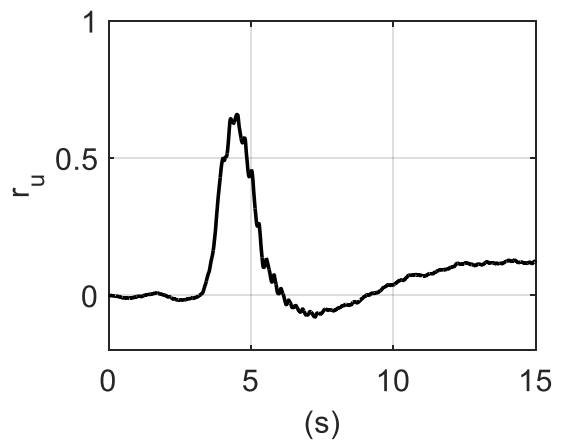


b. Pore-pressure ratio

Figure 4.15. Excess pore-pressure and pore-pressure ratio at 0.1 m depth (free-field - 1.5 Hz)



a. Excess pore-pressure



b. Pore-pressure ratio

Figure 4.16. Excess pore-pressure and pore-pressure ratio at 0.1 m depth (free-field - 2 Hz)

Figure 4.17 to Figure 4.19 show a window of the excess pore pressure plotted against shear strain for the three frequencies of loading. The window is situated in the plateau, where the excess pore pressure is cyclic in nature, but the mean shows little change. The shear strain was deduced from the relative displacement between two adjacent displacement transducers, situated outside the box at equivalent depths of 0.05m and 0.15m. The pore pressure transducer was situated at a depth of 0.1m, see Figure 4.4.

Two different types of responses were observed. For low frequency base motions, i.e. 1 Hz, a cyclic behaviour of the excess pore-pressure can be clearly seen. On the other hand, for high frequency (2 Hz) a near monotonic increase of the excess pore-pressure was recorded. This change in behaviour is similar to that discussed above in relation to Figure 4.14 to Figure 4.16. The dynamic properties of saturated cohesive and dry cohesionless soils are generally considered to be largely independent of frequency. This is also true for saturated but undrained cohesionless soils. This suggests the variation in behaviour seen here is due in part to the capacity for co-excitation drainage, which will decrease with increase in frequency.

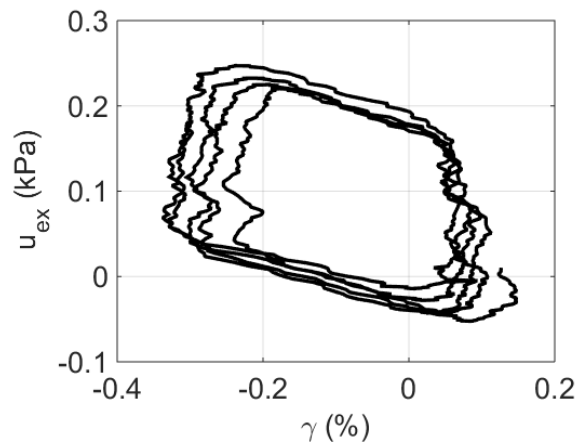


Figure 4.17. Excess pore-pressure v/s shear strain (%) at 0.1 m depth & 1 Hz (window from 7 to 12 s)

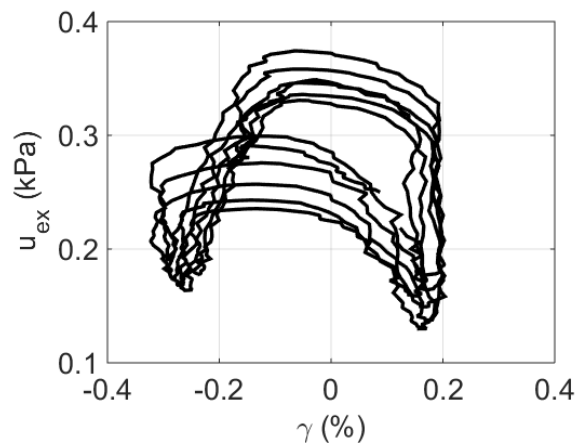


Figure 4.18. Excess pore-pressure v/s shear strain (%) at 0.1 m depth & 1.5 Hz (window from 6 to 10 s)

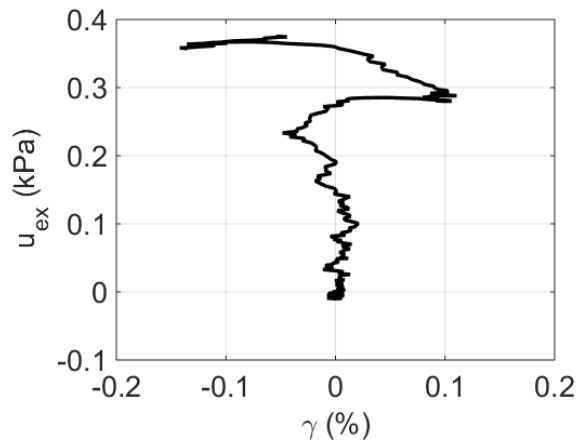


Figure 4.19. Excess pore-pressure v/s shear strain (%) at 0.1 m depth & 2 Hz (window from 2 to 5 s)

To further exemplify the two types of response observed, 3D representations of the dynamic pore-pressure as a function of time are presented in Figure 4.20 and Figure 4.21. In all “faces” on the figures (2 vertical walls and 1 horizontal floor) the corresponding 2D projections of the 3D graph are presented (grey images). Therefore, in the same graph the time evolution of both the dynamic pore-pressure and shear strain can be seen. The relationship between the pore-pressure and the shear strain is also presented.

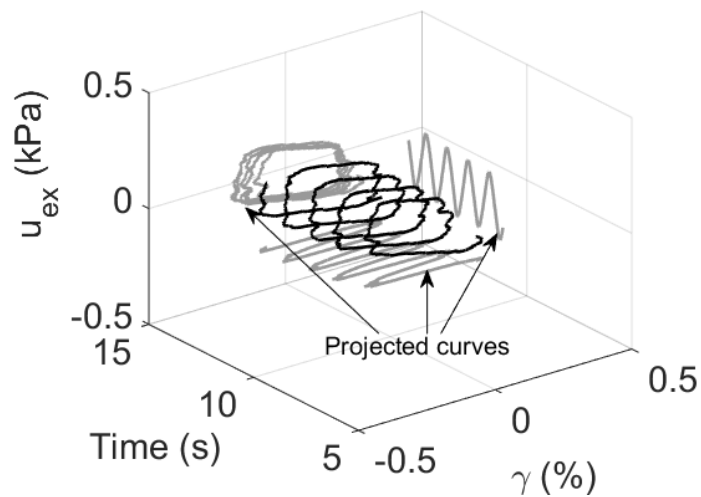


Figure 4.20. Time evolution of the pore-pressure in terms of the deformation index (1Hz)

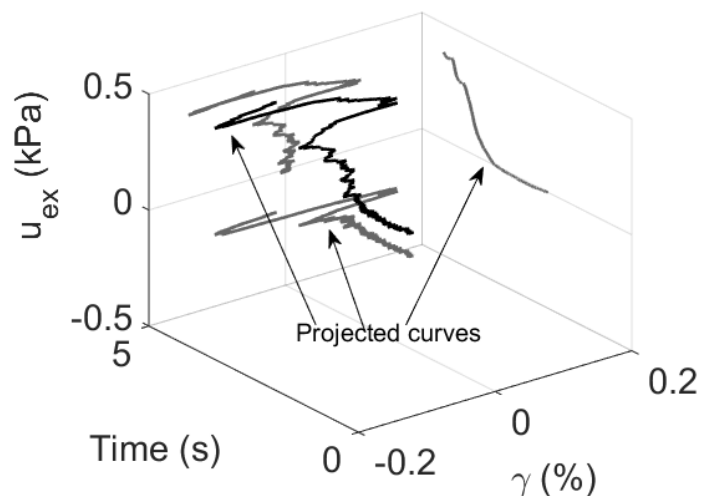


Figure 4.21. Time evolution of the pore-pressure in terms of the deformation index (2Hz)

One reason for the cyclic behaviour observed in Figure 4.20, compared to Figure 4.21, is that, in the case of Figure 4.20, the soil has more time to dissipate the excess of pore-pressure generated during each cycle, due to the lower frequency (1 Hz). This phenomenon is a direct effect of the frequency of the loading on the drainage capacity of the soil. On the other hand, Figure 4.21 shows a near monotonic increase in pore-pressure. In this case the larger frequency (2 Hz) does not allow the system to significantly dissipate the excess pore-pressure generated, producing a largely undrained response of the soil. This frequency dependant drained response cannot be observed in most of the classical geotechnical tests where the drainage condition is assumed a priori, and constrained by applying either a constant volume (undrained) condition or a quasi-static load (fully drained condition).

The co-excitation surface vertical displacement at the centre of the laminar box is presented in Figure 4.22 to Figure 4.24. The term “vertical displacement” is used since there is a cyclic component to the record, indicating recovery of some of the displacement. For the lowest frequency, Figure 4.22, the vertical displacement increases at a reasonably constant rate after the ramp at the beginning of the motion, while in the case of a 1.5 Hz motion there is a very rapid increase in vertical displacement following the initial ramp followed by a plateau of reasonably constant vertical displacement. The magnitude of the vertical displacement at the end of the motion in the case of the 1 Hz motion is approximately twice that of the 1.5 Hz motion. This reflects the co-excitation drainage in the 1 Hz case is greater than that of the 1.5 Hz. This can be further elucidated by observing that the gradient of the excess pore pressure with time following the motion is higher than that during the motion. This difference becomes more evident with increasing frequency. In the case of the 2 Hz excitation, the pore pressure is also shown on Figure 4.24 for comparison. It is evident that the pore pressure peaks at 5 seconds and decreases for the following 2.5 seconds while the displacement continues to increase, albeit marginally. There is little increase in displacement beyond 7.5 seconds, however, the pore pressure increases, probably as a result of fluid flow to the surface from below.

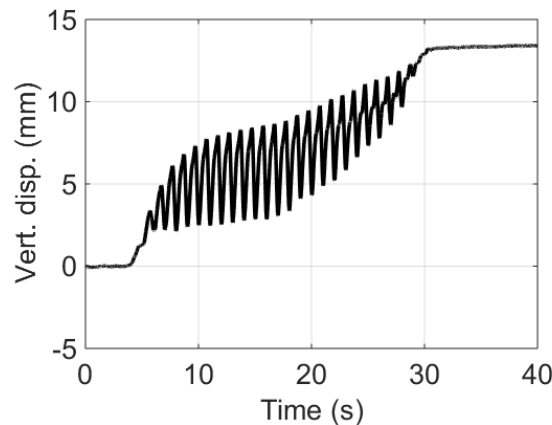


Figure 4.22. Surface settlement (free-field & 1 Hz)

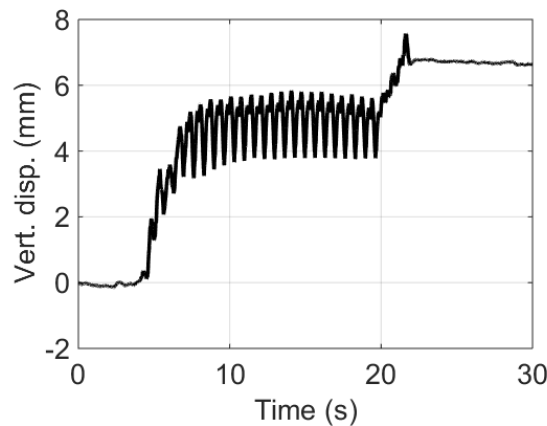


Figure 4.23. Surface settlement (free-field & 1.5 Hz)

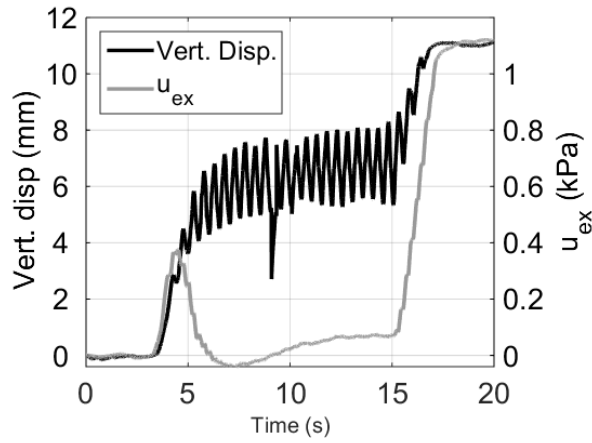


Figure 4.24. Surface settlement and excess pore-pressure at 0.1 m depth (free-field & 2 Hz)

Recorded ground motion

Harmonic base motions allow the opportunity to study particular accelerations and frequencies; however, earthquakes shaking is a mixture of different frequencies and amplitudes and thus is much more complex. A recorded ground motion from the Darfield earthquake, Rakaia School station (see Table 4.3) was used to study the response of the sand. Because we are studying a deposit of sand (although it is less than 1.5 m in depth) a ground motion recorded on soil was specifically selected.

The excess pore-pressure resulting from the earthquake loading is presented in Figure 4.25, Figure 4.26 and Figure 4.27 for depths of 0.1m 0.7 m and 1.35 m, respectively. The pore-pressure ratio is also presented.

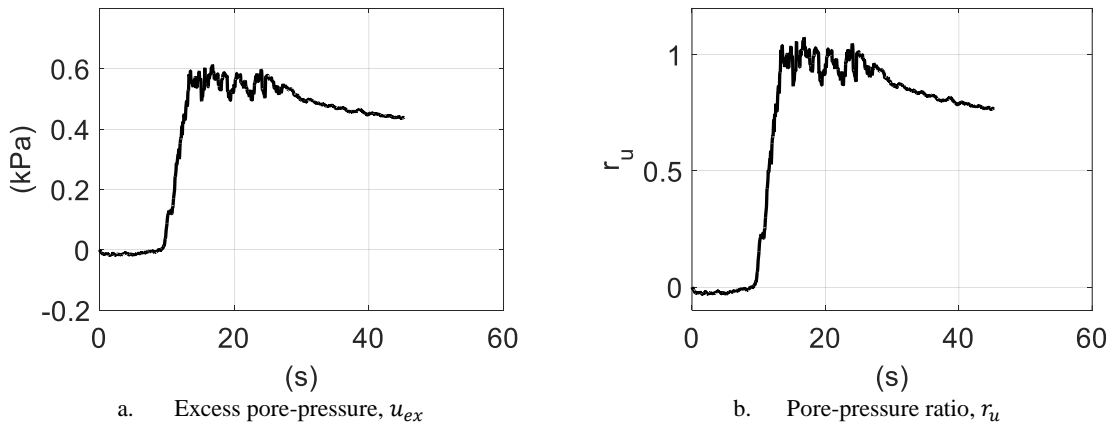


Figure 4.25. Excess pore-pressure and pore-pressure ratio at 0.1 m depth (RKAC)

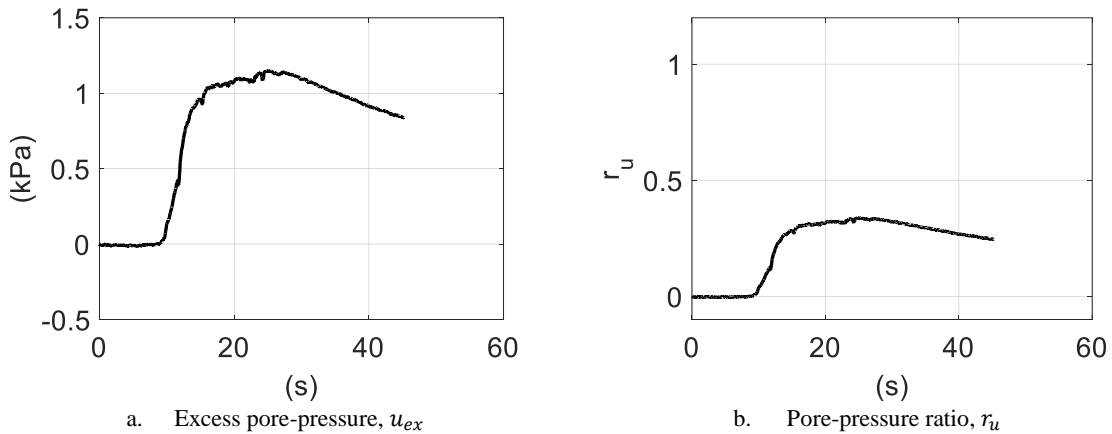


Figure 4.26. Excess pore-pressure and pore-pressure ratio at 0.7 m depth (RKAC)

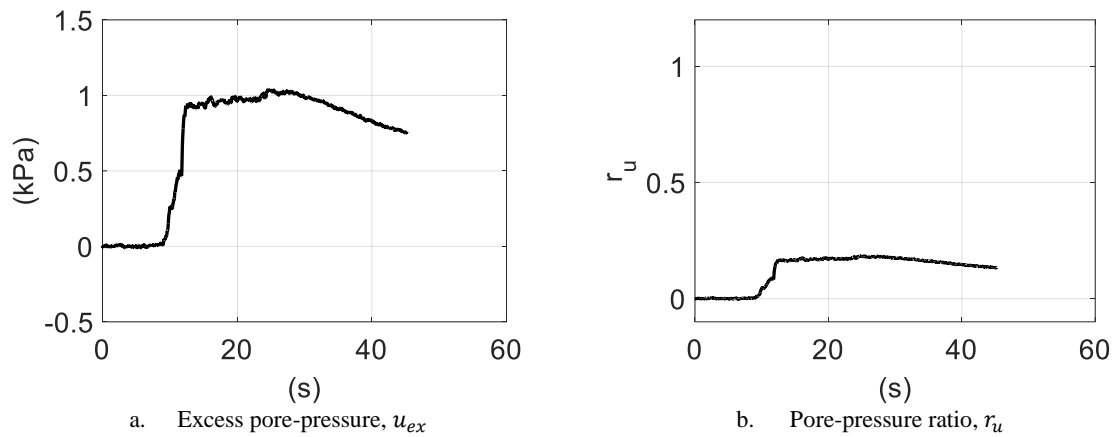


Figure 4.27. Excess pore-pressure and pore-pressure ratio at 1.35 m depth (RKAC)

All the dynamic pore-pressure records from the recorded earthquake motion are considerably smoother than those from the harmonic base motions. The difference is due to the larger amplitude of the harmonic-induced shear strain, and the number of cycles, applied to the sand, compared to a multi-frequency transient seismic motion. Liquefaction was recorded close to the surface (0.1 m depth, see Figure 4.25). The excess pore-pressure at this depth reached a value close to 0.6 kPa, which corresponds to the initial effective vertical stress (σ'_{v0}). This can also be observed in Figure 4.25-b.

The excess pore pressure in terms of shear strain at a depth of 0.1 m is presented in Figure 4.28. Here liquefaction can also be observed where the excess pore-pressure remains close to 0.6 kPa for some considerable time. The rapid path to liquefaction can also be seen, involving only a few cycles to reach the maximum excess pore-pressure.

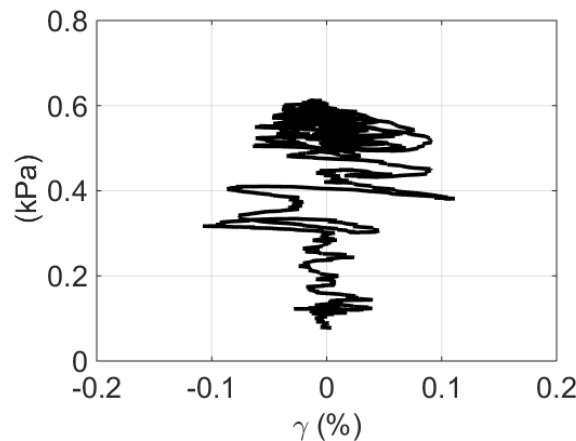


Figure 4.28. Excess pore-pressure v/s shear strain for RKAC ground motion

4.3.2 Effects of footings

When introducing footings into the experiments there is an increase in vertical effective stress in the soil beneath the footings. The contact stress for a single footing has been given as 1.93 kPa in Section 4.2.3. This stress is small, and it will attenuate with depth. For this reason the near surface zone, approximately the upper few hundred millimetres, is the focus of attention when considering the response of footings.

The single footing will impart both horizontal shear and moment to the sand. The footing has no superstructure attached, thus it is likely that the major part of the SSI will result from the transfer of horizontal shear to the sand. The resulting generation of excess pore pressure can be considered to result from the arrival and reflection of alternating shear stress from wave propagation (SH waves), plus the SSI effect of an alternating surface shear traction (and moment) from the footing. In the case of the six-cluster, the emerging waves from the adjacent footings will create a complex wave field of compression, shear and surface waves in addition to the body waves describe above. If there are significant excess pore pressures developed the sand will be responding, at least over some part of the excitation, in a nonlinear manner. Shear, normal and volumetric strains will develop which will affect the permeability of the sand, especially in the near surface region of low effective stress.

Harmonic loads

A maximum acceleration of 0.2 g and 20 cycles (of maximum amplitude) were utilised for all harmonic loading involving the footings (Table 4.3). Frequencies of 1, 1.5 and 2 Hz were applied. The dynamic pore-pressures 0.1 m beneath the centre of the footing for the stand-alone, and for the cluster of six footings, are presented in Figure 4.29. Only the shallowest pore-pressure device is presented because no major influence of the footing/footings was observed in the deeper devices. Horizontal dashed lines represent the maximum pore pressure for the corresponding free-field case.

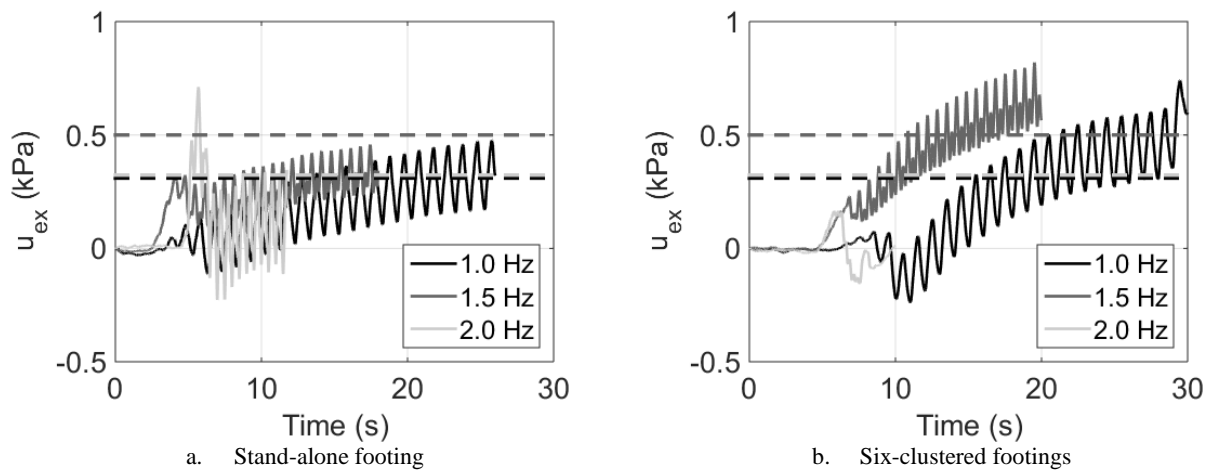


Figure 4.29. Excess pore-pressure 0.1 m beneath the centre of the footing/footings

For the stand-alone case, Figure 4.29-a, similar free field excess pore-pressure to that of the 1 Hz excitation. On the other hand, for the cluster of six footings, Figure 4.29-b shows a larger excess pore-pressure than that of the free field for both the 1 and 1.5 Hz excitations. The increase in the pore-pressure due to the presence of a footing has been observed in centrifuge tests (Marques, et al. 2012) and numerical analyses (Lopez-Caballero and Modaressi 2008). The results of this study show similar trends, albeit with a much lower bearing pressure than those considered for the centrifuge and numerical work.

The dynamic pore-pressure at 0.05 m depth in relation to the shear strain is presented in Figure 4.30, Figure 4.31 and Figure 4.32 for 1, 1.5 and 2 Hz, respectively. Both configurations, i.e. stand-alone and the six-clustered footings) are presented. The response for the free-field case is presented in grey dashed line as a reference. For the six-clustered case the reading was obtained from beneath the centre of the array of footings, as is shown in Figure 4.4.

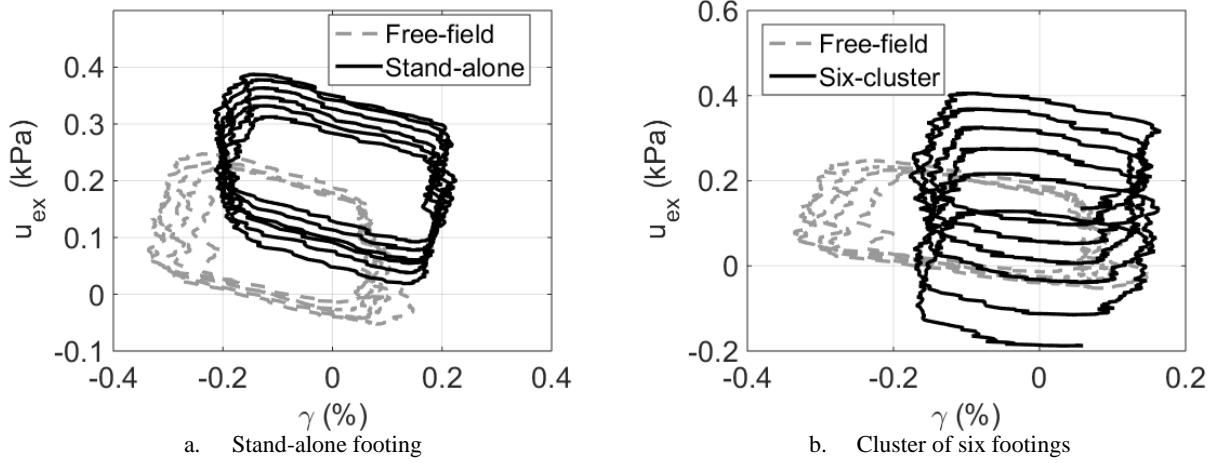


Figure 4.30. Excess pore-pressure v/s shear strain at 0.1 m depth beneath the footings (1 Hz)

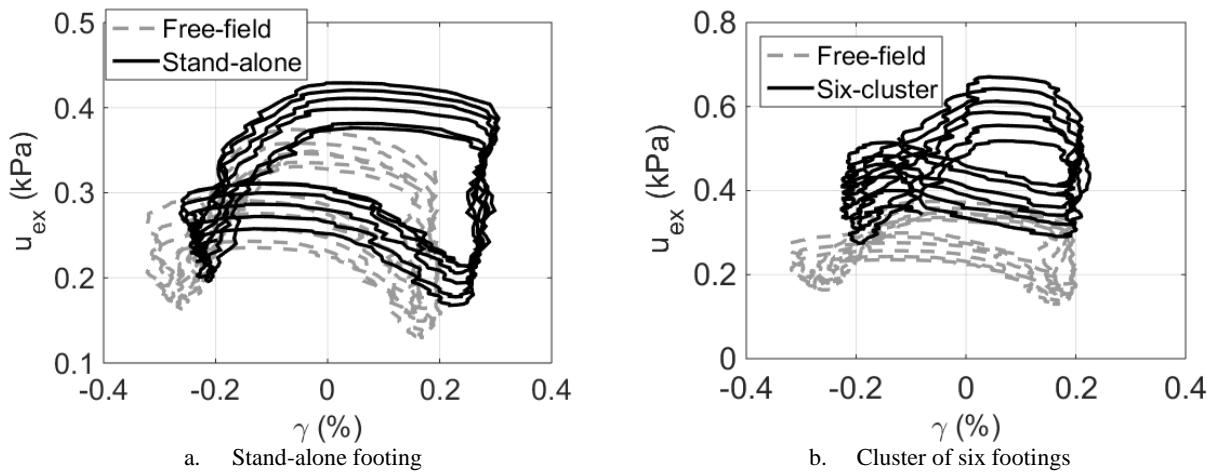


Figure 4.31. Excess pore-pressure v/s shear strain at 0.1 m depth beneath the footings (1.5 Hz)

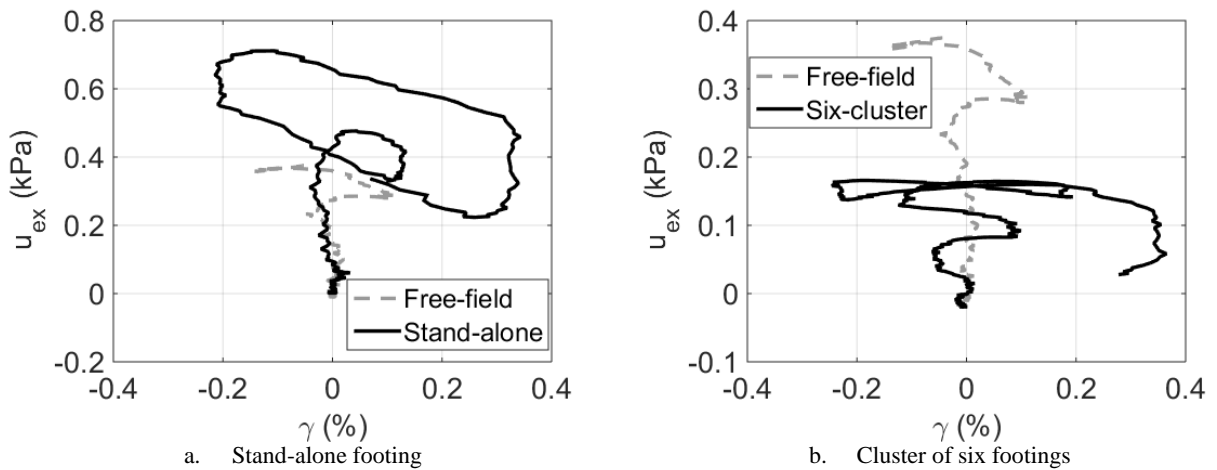


Figure 4.32. Excess pore-pressure v/s shear strain at 0.1 m depth beneath the footings (2 Hz)

The different nature of the excess pore pressure as a function of the shear strain and frequency may be seen. The presence of the footing/footings increases the maximum pore pressure compared to the free field in almost all cases (except the 2 Hz six-cluster), and it is evident to an increased degree for the six-cluster. The global behaviour is similar in all cases to the free field.

All the six-cluster records show the effect of restricted drainage compared with the stand-alone records. The spreading of the loops indicates the growth of excess pore pressure with time from the rate of generation of excess pore pressure exceeding the rate of dissipation. The excess pore-pressure for all cases, except the six-cluster 2 Hz, involving footings (black solid lines) are larger than the corresponding free-field case (dashed grey lines).

Figure 4.33 shows the maximum acceleration of the footing/footings (a_f) divided by the corresponding maximum acceleration of the table (a_t). Use of this quotient is intended to eliminate the influence of the unwanted small differences in the acceleration of the table between tests. Figure 4.33-a shows all footings while Figure 4.33-b shows the average of all footings corresponding to each test.

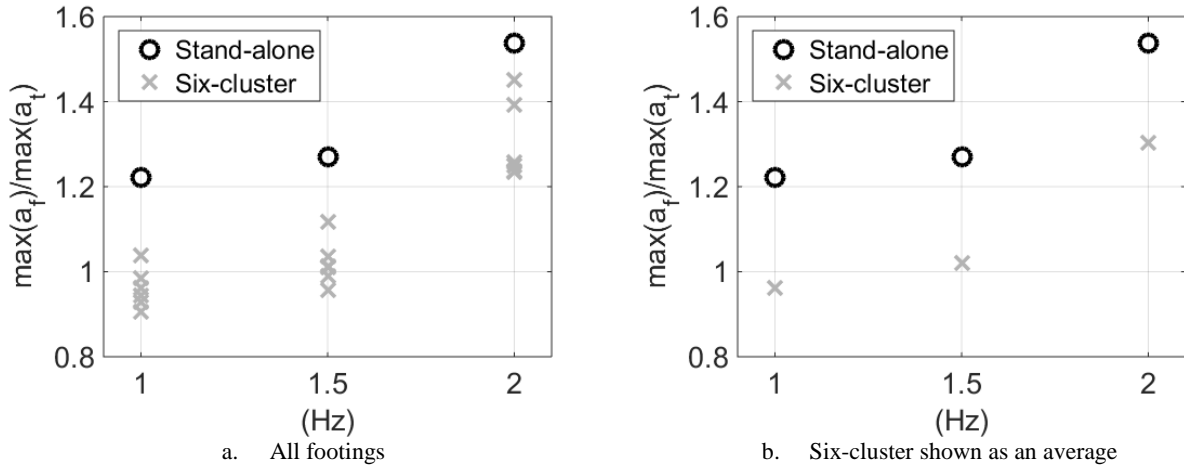


Figure 4.33. Ratio of the maximum acceleration of the footings to the maximum of the table

The acceleration of the stand-alone footing was higher across all frequencies compared to that of the cluster of six footings. However, both cases presented an increasing maximum acceleration with increasing frequency. The data strongly supports concluding that the effect of clustering reduces the acceleration experienced by the footings compared with a stand-alone footing. This may be due to destructive interference in the wave field of the cluster. For any given frequency, the accelerations and hence the displacement (leading to pore pressure generation) of the six cluster is lower than that of the stand-alone footing. However the excess pore pressure is generally higher. This implies the rate of dissipation of excess pore pressure in the case of the six-cluster is lower than that of the stand-alone footing. This is probably related to the length of the drainage path due to the closely adjacent spacing of footings in the cluster. In the real case of shoulder to shoulder buildings on a single foundation this effect would be amplified.

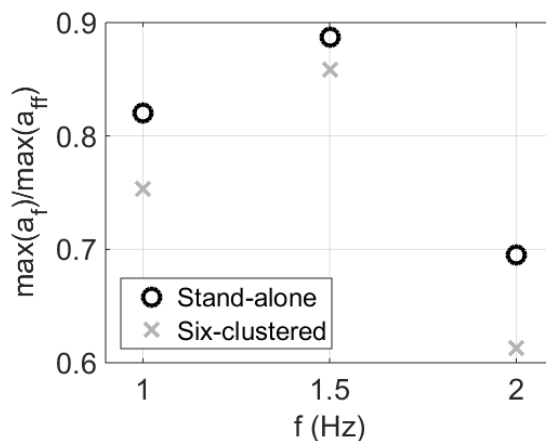


Figure 4.34. Ratio of the maximum acceleration at the footings to that of the free-field

Figure 4.34 shows the ratio of the maximum acceleration recorded at the footings to that of the free-field. For the case of six-clustered footings the average of all the footings is presented. All the cases presented values lower than one, and implies that the acceleration recorded on the footings was lower than that for the free-field. The lower acceleration recorded for the cluster of footings compared to the stand-alone footing is also evident.

Another highly relevant parameter in the design of footings on saturated sand is the vertical displacement due to earthquake loads. This is presented in Figure 4.35 to Figure 4.37 for the different frequencies. In the case of six-clustered footings only one result (the centre footing) is presented for simplicity. The six-clustered case presented a lower settlement for the low-frequency (1 Hz) case (Figure 4.35) compare to that from the stand-alone case. The 1.5 Hz (Figure 4.36) case presented similar settlement for both a stand-alone and the six-cluster. The larger frequency (2 Hz) presented a higher settlement for the six-clustered models (Figure 4.37). These results convey the influence of both the number and configuration of the footings and the frequency content of the loading. A possible reason for the differences in the settlement is that for a low frequency there is a lower excess pore-pressure generation compared to that for the higher frequency load. Therefore, the initial vertical stress due to the presence of several footings generates a stiffer soil response under a low-frequency load. However, a larger settlement under a high-frequency load results from the larger excess pore-pressure, which on dissipation produces a larger settlement.

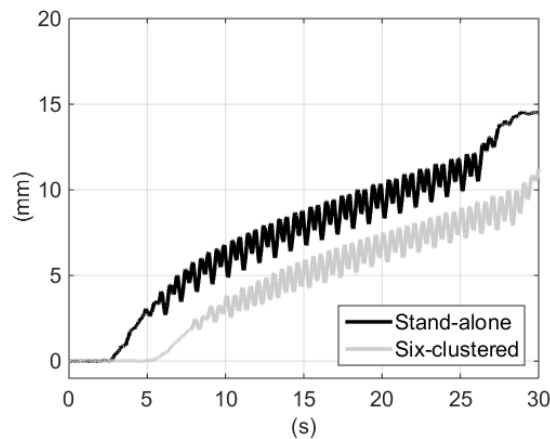


Figure 4.35. Footings settlement for harmonic loads (1 Hz)

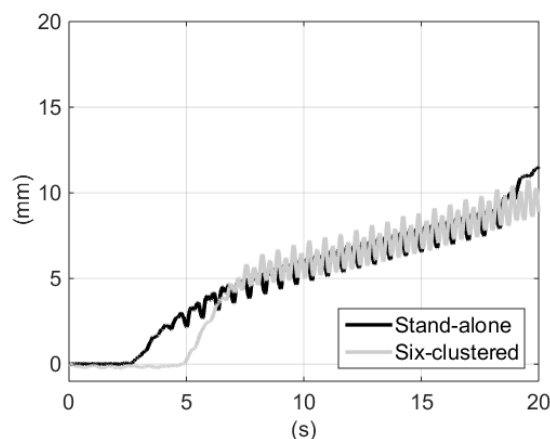


Figure 4.36. Footings settlement for harmonic loads (1.5 Hz)

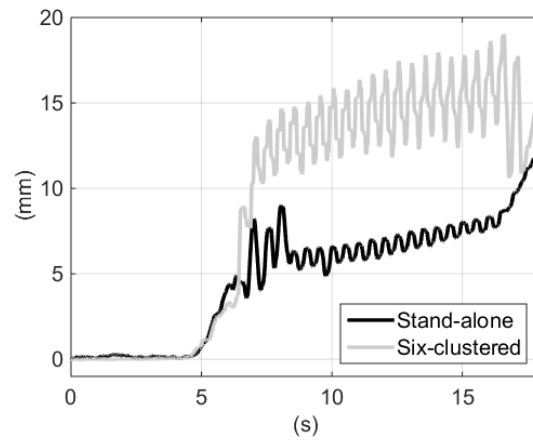


Figure 4.37. Footings settlement for harmonic loads (2 Hz)

Recorded ground motion

Figure 4.38 shows the dynamic pore-pressure at 0.1 m depth in terms of the shear strain. The results for the free-field case are also presented as a grey dashed line. Both cases (stand-alone and six-clustered) presented a similar level of final excess pore-pressure which was higher than that of the free-field. It can also be seen that the level of maximum strain in the case of the stand-alone footing is a factor of three higher than the six-cluster. This could be caused, at least in part, by the destructive interference of the individual wave fields from each of the six footings, leading to a lower integrated response.

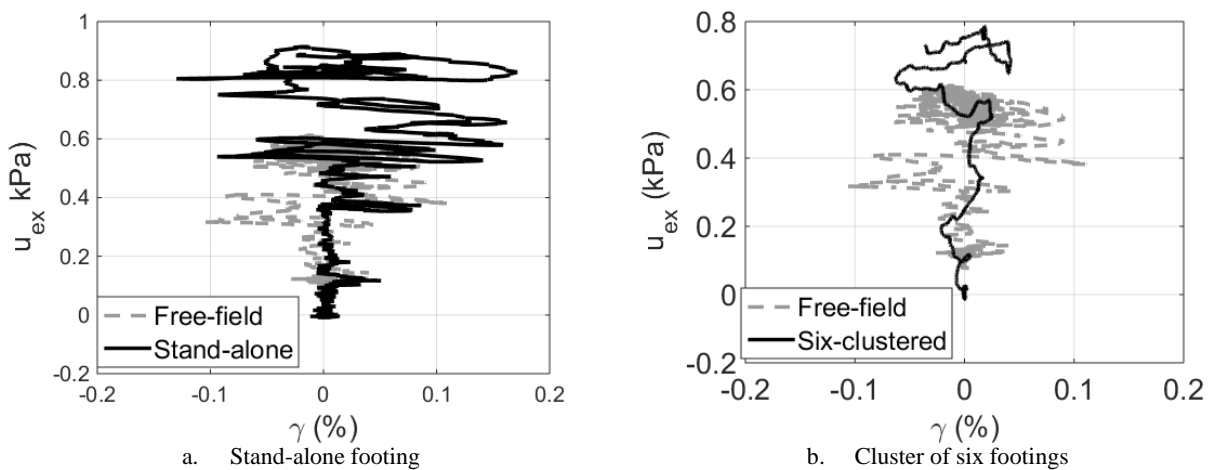


Figure 4.38. Excess pore-pressure and shear strain at 0.1 m beneath the centre of the footings (RKAC)

The value of a_f/a_t for the footings cases subjected to the recorded ground motion (RKAC) was also evaluated. The corresponding value was 1.02 for the stand-alone condition and 0.64 for the six-clustered models. As was observed for the harmonic loads (Figure 4.33), the stand-alone case presented a larger acceleration.

5 CONCLUSIONS

To have improved insight into the response of shallow footings on saturated and dry cohesionless soil under dynamic loads, the following tasks were conducted:

- (i) A large laminar box was built to closely simulate the soil deformation under dynamic loads. This box can be used to study both non-saturated and saturated soils.
- (ii) A set of tests considering different configurations of shallow footings on saturated soil were performed. Harmonic loads and a record of a recorded earthquake ground motion were used.

The main observations from this work are presented below.

1. A large laminar box was designed and constructed capable of simulating the earthquake deformation of saturated soil media.
2. Subsurface excess pore-pressure and acceleration were successfully measured for harmonic loading (3 frequencies – 1, 1.5 and 2 Hz) as well as a recorded seismic ground motion for 3 cases;
 - a. The free field
 - b. A stand-alone footing
 - c. A cluster of 6 closely adjacent footings.
3. Since, in a general sense, the recorded settlement of the footings in this study is different from that of the free field, it has become apparent that current free field methods should not be used for estimating the settlement of footings. On a fundamental level this is apparent due to the different underlying mechanisms of the two cases.
4. This study was performed using sand at a $D_r \approx 50\%$ with a permeability estimated to be $k = 2.2 \times 10^{-3}$ m/s. There is clear evidence of co-seismic drainage of near surface excess pore-pressure during the passage of the earthquake, as well as after the termination of the motion.
5. There are circumstances (e.g. particularly near surface loose sand) where it is not realistic to consider the sand to behave in an undrained manner.
6. The footings configuration was observed to play a significant role in the response of the soil-footings system.
 - a. The data shows that the number of footings and the frequency of loading significantly affects the net effect of the generation and diffusion of excess pore-pressure.
 - b. The larger the foot-print of the footings the more undrained the observed response. The same trend was observed with increasing frequency.
 - c. The rate of generation of excess pore-pressure and the rate of diffusion were both different for the cases of a single footing and a cluster of six closely spaced footings. These 2 effects, i.e. pore pressure generation and dissipation, cannot be quantitatively separated in this work.

7. In this study there was evidence that the acceleration associated with both a stand-alone and a closely adjacent cluster of footings is less than that of the free field. However, considering the uncertainties in seismic design, in the view of the authors, this difference is not sufficient to routinely reduce the free field motion for the seismic design of shallow foundations on saturated sandy soil.
8. The number of footings and the frequency of loading both affects the co-seismic settlement of a footing. The presence of a footing: (1) changes the pre-seismic effective stress regime and hence the shear modulus; and (2) the drainage conditions with regard to the excess pore-pressure.
9. The complex combined effects of both the number of footings and the frequency content of the loading were observed to affect highly the settlement of shallow footings.
 - a. For a low frequency loading (1 Hz) the stand-alone footing presented a larger co-seismic settlement compared to the six-clustered footings. This can be related to the larger increase in effective stress for a larger number of footings combined with the lower excess pore-pressure generated.
 - b. For a large frequency (2 Hz) the opposite trend was observed, i.e. the cluster of footings experienced a larger settlement compared to that for the stand-alone condition. In this case the cluster of footings presented a monotonic increase of the excess pore-pressure in contrast to the cyclic pore-pressure observed for the stand-alone footing (see Figure 4.32).

6 RECOMMENDATIONS

Based on the main observations from this study, the following recommendations regarding shallow footings in sand under seismic loading are proposed.

1. It is necessary to include the effects of footings when estimating settlement induced by seismic loading on saturated sand.
2. Rather than considering the sand as acting in an undrained fashion, engineers would benefit from considering, on the basis of relative density, permeability and the characteristics (strength, frequency, etc.) of the earthquake loading, that the sand will behave in a partially drained manner.
3. To obtain a more reliable estimation of footing seismic response, the configuration of footings (i.e. number and location) and the characteristics of the loading need to be considered.
4. The practice of routinely reducing the free-field acceleration for estimation the footing acceleration should be discontinued. Instead, the characteristics of the soil-footings system must be taken into account.

7 PUBLICATIONS AND PUBLIC DISSEMINATION

7.1 PhD theses

1. Barrios, G. (2018) Seismic behaviour of clustered structures in liquefiable soil, *PhD Thesis*, University of Auckland, <https://researchspace.auckland.ac.nz/handle/2292/1/discover>.
2. Qin, X. (2016) Experimental studies of SFSI effect on upliftable structures, *PhD Thesis*, University of Auckland, ResearchSpace, Auckland, New Zealand, <https://researchspace.auckland.ac.nz/handle/2292/29301>.

7.2 Journal articles

1. Qin, X., Chouw, N. (2017) Shake table study on the effect of mainshock-aftershock sequences on structure with SFSI, *Shock and Vibration*, ID 9850915, 12 pages, <https://doi.org/10.1155/2017/9850915>
2. Barrios, G., Larkin, T., Chouw, N. (under review) Influence of shallow footings on the dynamic response of saturated sand with low confining pressure.

7.3 Conference papers

1. G. Barrios, X. Qin, T. Larkin, N. Chouw (2018) Impact of liquefied soil on shallow footings, *16th European Conference on Earthquake Engineering*, 18-21 June, Thessaloniki, Greece.
2. G. Barrios, X. Qin, T. Larkin, N. Chouw (2018) Seismic behaviour of clustered structures in liquefiable soil, *15th International Symposium on Structural Engineering*, Zhejiang, China.

7.4 Knowledge transfer through teaching activities

Final-year projects

Two undergraduate students were directly involved in the research as part of their final-year project entitled “Seismic performance of clustered structures in earthquakes”.

Post-graduate level course

Some of the research outcomes will be discussed in the course Civil710 – “Advanced structural dynamics”. Students will be involved in the lab activities to simulate and to understand the seismic performance of structure-footing-soil systems.

7.5 Public seminars

To disseminate the research outcomes to end-users a whole day seminar on “Seismic performance of structure–foundation–soil systems” was presented, with discussion sessions, in Wellington, Nelson, Christchurch and Auckland.

The objective was to transfer understanding, from the insights obtained from the research work, to practicing engineers.

Participants attended the seminars, representing:

Christchurch City Council,
Forbes Consultants,
Ashby Consulting Ltd,
CLC Consulting Group,
KGA Geotechnical Group Ltd,
Tonkin + Taylor,
Soil + Rock Consultants,
Markplan Consulting Ltd,
MTL Civil LTD,
Structural Sense,
Structus,
Engineering Design Consultants Ltd, Haigh Workman,
GDC Consultants,
Riley Consultants,
Hiway Geotechnical,
Beca, BCD Group Ltd,
Kevin O’Connor & Associates Ltd,
E. Holt Ltd,
Compusoft Engineering Ltd,
Mainmark Ground Engineering,
Holmes Consulting Group,
Aurecon NZ Ltd,
Batchelar McDougall Consulting Eng.,
Miyamoto International,
Opus International Consultants,
Geotech Consulting Ltd,
Stantec,
NZET Consulting Engineers Ltd,
Calibre Consulting Ltd,
Jacobs Engineering Ltd,
Resource Development Consultants Ltd,
TSE Taranaki & Associates Ltd,
Coffey Services NZ Ltd,
Sawrey Consulting Engineers,
ETS Engineers Ltd,
Davidson Group,
CGW Consulting Engineers.

REFERENCES

- Buckingham, E. 1914. "On physically similar systems; illustrations of the use of dimensional equations." *Physical review (APS)* 4 (4): 345.
- Cheung, W M, X Qin, N Chouw, T Larkin, and R Orense. 2013. "Experimental and numerical study of soil response in a laminar box." *Proceeding of 2013 NZSEE Conference*.
- Chopra, Anil K, and Solomon C-S Yim. 1985. "Simplified earthquake analysis of structures with foundation uplift." *Journal of Structural Engineering (American Society of Civil Engineers)* 111 (4): 906-930.
- Chouw, N and H Hao. 2005. "Study of SSI and non-uniform ground motion effect on pounding between bridge girders." *Soil Dynamics and Earthquake Engineering (Elsevier)* 25 (7): 717-728.
- Hazen, A. 1930. "Water supply." *American Civil Engineers Handbook (John Wiley & Sons New York)* 1444-1518.
- Hyodo, M, A F L Hyde, N Aramaki, and Y Nakata. 2002. "Undrained monotonic and cyclic shear behaviour of sand under low and high confining stresses." *Soils and Foundations (The Japanese Geotechnical Society)* 42 (3): 63-76.
- Idriss, I M, and R W Boulanger. 2008. *Soil liquefaction during earthquakes*. Earthquake Engineering Research Institute.
- JSCE. 2000. *Earthquake Resistant Design Codes In Japan*, Tokyo, Maruzen.
- Larkin, T J. 1978a. "DENSOR, A computer program for seismic response analysis of non linear horizontal soil layers." *Norwegian Geotech. Inst., Internal Report 51508-6*.
- Larkin, T J. 1978b. "Nonlinear effective stress dependent site response of horizontal soil media." *Norwegian Geotechnical Inst., Internal report 51508-7*.
- Larkin, T. 2008. "Seismic response of liquid storage tanks incorporating soil structure interaction." *Journal of Geotechnical and Geoenvironmental Engineering (American Society of Civil Engineers)* 134 (12): 1804-1814.
- Latha, G M, and A M Krishna. 2008. "Seismic response of reinforced soil retaining wall models: influence of backfill relative density." *Geotextiles and Geomembranes (Elsevier)* 26 (4): 335-349.
- Lopez-Caballero, F, and A Modaressi. 2008. "Numerical simulation of liquefaction effects on seismic SSI." *Soil Dynamics and Earthquake Engineering (Elsevier)* 28 (2): 85-98.
- Madhav, M R, and A Khrishna. 2008. "Liquefaction mitigation of sand deposits by granular piles-an overview." In *Geotechnical Engineering for Disaster Mitigation and Rehabilitation*, 66-79. Springer.
- Marques, A, P A L F Coelho, U Cilingir, S K Haigh, and G Madabhushi. 2012. "Earthquake-induced liquefaction effects on a shallow foundation." *WCEE Conference*.
- Matuo, H and S Ohara. 1976. "Lateral earth pressure and stability of quay walls during earth-quakes." *Technology Reports of the Yamaguchi University*. 455-466.
- MBIE. 2016. *Earthquake geotechnical engineering practice, Module 3: Identification, assessment and mitigation of liquefaction hazards*.
- Mononobe, N, and O Matsuo . 1929. "On determination of earth pressure during earthquake." *Proc. of the World Engrg. Congress, Tokyo, 1929*, 177-185.
- Mori, K, K Sakai, A Mori, and R Orense. 1997. "New methods for better predicting soil behavior under earthquake loading." *Proceedings of the International Conference on Soil Mechanics and Foundation Engineering*. AA Balkema. 163-166.
- Motamed, R, I Towhata, T Honda, K Tabata, and A Abe. 2013. "Pile group response to liquefaction-induced lateral spreading: E-Defense large shake table test." *Soil Dynamics and Earthquake Engineering (Elsevier)* 51: 35-46.
- Okamoto, M, and S Fityus. 2006. "An evaluation of the dry pluviation preparation technique applied to silica sand samples." *Geomechanics and Geotechnics of Particulate Media: Proceedings of the International Symposium on Geomechanics and Geotechnics of Particulate Media*. Taylor and Francis, London. 33-34.

- Orense, R, S Yasuda, I Morimoto, and M Takagi. 2001. "Full-scale shaking table tests on the behavior of piles during earthquakes." *Proceedings of the Second Japan Philippines Workshop on Safety and Stability of Infrastructure against Environmental Impacts*. Manila, Philippines. 159-168.
- Pitilakis, D, M Dietz, D Muir Wood, D Clouteau, and A Modaressi. 2008. "Numerical simulation of dynamic soil-structure interaction in shaking table testing." *Soil Dynamics and Earthquake Engineering* 28 (6): 453-467.
- Prasad, S K, I Towhata, G P Chandradhara, and P Nanjundaswamy. 2004. "Shaking table tests in earthquake geotechnical engineering." *Current Science (JSTOR)* 1398-1404.
- Qin, X. 2016. *Experimental studies of SFSI effect on upliftable structures*. (Doctoral dissertation, Auckland, New Zealand): <https://researchspace.auckland.ac.nz/handle/2292/29301>.
- Qin, X, W M Cheung, N Chouw, T Larkin, and S W C Ching. 2013. "Study of soil-structure interaction effect on ground movement using a laminar box." *Proceeding of 2013 NZSEE Conference*. Wellington, New Zealand.
- Rad, N S, and M T Tumay. 1987. "Factors affecting sand specimen preparation by raining." (ASTM International).
- Sato, M, and K Tabata. 2010. *Study on reproduction procedure of E-Defense large-scale soil tests evaluated by dynamic centrifuge modelling -Tests on dynamic soil-pile-structure interaction in horizontal sand deposit*. Report of the National Research Institute for Earth Science and Disaster Prevention, 33-42.
- Seed, R B, K O Cetin, RES Moss, AM Kammerer, J Wu, JM Pestana, MiF Riemer, et al. 2003. "Recent advances in soil liquefaction engineering: a unified and consistent framework." *Proceedings of the 26th Annual ASCE Los Angeles Geotechnical Spring Seminar: Long Beach, CA*.
- Taylor, P W, P E Bartlett, and P R Wiessing. 1980. "Foundation rocking under earthquake loading." *Proc. Tenth International Conference on Soil Mechanics and Foundation Engineering*. Stockholm: 313-322.
- The Overseas Coastal Area Development Institute of Japan and Ports and Harbours Bureau, Ministry of Land, Infrastructure, Transport and Tourism and National Institute for Land and Infrastructure Management and Port and Airport Research Institute. 2009. *Technical Standards and Commentaries for Port and Harbour Facilities in Japan*. Overseas Coastal Area Development Institute of Japan.
- Turan, A , S D Hinchberger, and H El Naggar. 2009. "Design and commissioning of a laminar soil container for use on small shaking tables." *Soil Dynamics and Earthquake Engineering* (Elsevier) 29 (2): 404-414.
- Ueng, TS. 2010. "Shaking table tests for studies of soil liquefaction and soil-pile interaction." *Geotechnical Engineering* 41 (1): 29.
- Ueng, TS, MH Wang, MH Chen, CH Chen, and LH Peng. 2005. "A large biaxial shear box for shaking table test on saturated sand." (ASTM International).
- Vaid, Y P , and D Negussey. 1984. "Relative density of pluviated sand samples." *Soils and Foundations* (The Japanese Geotechnical Society) 24 (2): 101-105.
- Veletsos, AS, and JW Meek. 1974. "Dynamic behaviour of building-foundation systems." *Earthquake Engineering & Structural Dynamics* (Wiley Online Library) 3 (2): 121-138.
- Yasuda, S, K Ishihara, I Morimoto, R Orense, M Ikeda, and S Tamura. 2000. "Large-scale shaking table tests on pile foundations in liquefied ground." *Proc., 12th World Conf. on Earthquake Engineering*.
- Youd, T L, I M Idriss. 2001 et al. "Liquefaction resistance of soils: summary report from the 1996 NCEER and 1998 NCEER/NSF workshops on evaluation of liquefaction resistance of soils." *Journal of Geotechnical and Geoenvironmental Engineering* (American Society of Civil Engineers) 127 (4): 297-313.